Molecular and Cellular Biology

Higher-Order Chromatin Regulation and Differential Gene Expression in the Human Tumor Necrosis Factor/Lymphotoxin Locus in Hepatocellular Carcinoma Cells

Takehisa Watanabe, Ko Ishihara, Akiyuki Hirosue, Sugiko Watanabe, Shinjiro Hino, Hidenori Ojima, Yae Kanai, Yutaka Sasaki and Mitsuyoshi Nakao

Mol. Cell. Biol. **2012, 32(8):1529. DOI: 10.1128/MCB.06478-11.**
Published Ahead of Print 21 February 2012.

MCB
Journals.ASM.org

Higher-Order Chromatin Regulation and Differential Gene Expression in the Human Tumor Necrosis Factor/Lymphotoxin Locus in Hepatocellular Carcinoma Cells

Takehisa Watanabe,[a,b] Ko Ishihara,[c,e] Akiyuki Hirosue,[a] Sugiko Watanabe,[a] Shinjiro Hino,[a] Hidenori Ojima,[d] Yae Kanai,[d] Yutaka Sasaki,[b] and Mitsuyoshi Nakao[a,e]

Department of Medical Cell Biology, Institute of Molecular Embryology and Genetics, and the Global Center of Excellence Cell Fate Regulation Research and Education Unit,[a] Department of Gastroenterology and Hepatology, Graduate School of Medical Sciences,[b] and Priority Organization for Innovation and Excellence,[c] Kumamoto University, Kumamoto, Japan; Division of Molecular Pathology, National Cancer Center Research Institute, Tokyo, Japan[d]; and Core Research for Evolutional Science and Technology (CREST), Japan Science of Technology Agency, Tokyo, Japan[e]

The three-dimensional context of endogenous chromosomal regions may contribute to the regulation of gene clusters by influencing interactions between transcriptional regulatory elements. In this study, we investigated the effects of tumor necrosis factor (TNF) signaling on spatiotemporal enhancer-promoter interactions in the human *tumor necrosis factor* (*TNF*)/*lymphotoxin* (*LT*) gene locus, mediated by CCCTC-binding factor (CTCF)-dependent chromatin insulators. The cytokine genes *LTα*, *TNF*, and *LTβ* are differentially regulated by NF-κB signaling in inflammatory and oncogenic responses. We identified at least four CTCF-enriched sites with enhancer-blocking activities and a TNF-responsive TE2 enhancer in the *TNF/LT* locus. One of the CTCF-enriched sites is located between the early-inducible *LTα/TNF* promoters and the late-inducible *LTβ* promoter. Depletion of CTCF reduced *TNF* expression and accelerated *LTβ* induction. After TNF stimulation, via intrachromosomal dynamics, these insulators mediated interactions between the enhancer and the *LTα/TNF* promoters, followed by interaction with the *LTβ* promoter. These results suggest that insulators mediate the spatiotemporal control of enhancer-promoter associations in the *TNF/LT* gene cluster.

Chromosomal regions harboring different tissue-specific or cellular-state-specific gene clusters may be influenced by long-range regulatory elements and higher-order chromatin organization (45, 53, 60). Recent studies suggest that transcriptional regulatory elements, such as enhancers, promoters, and chromatin insulators, contribute to gene activation and inactivation via genome accessibility and chromosomal interactions (8, 18). Among these, chromatin insulators are boundary elements that partition the genome into chromosomal subregions, probably through their ability to block interactions between enhancers and promoters when positioned between them (enhancer-blocking effect) (7, 17, 41). However, the precise mechanisms responsible for the enhancer-blocking effect and the relationship with long-range chromatin interactions remain unclear (47, 49). The CCCTC-binding factor CTCF is a highly conserved 11-zinc-finger protein that plays crucial roles at insulator sites (44). CTCF is also reported to function in transcriptional activation (62, 73) and repression (16, 36). In the *IGF2/H19* locus, CTCF binds to the differentially methylated region (DMR) of the *H19* gene to form a predicted chromatin loop structure (6, 22, 42). Genome-wide analyses identified the distribution of the putative CTCF-binding sites and their consensus sequences (4, 27, 28, 69). We and other groups recently determined that CTCF is enriched with cohesin in at least 14,000 sites on the human genome (46, 54, 65). CTCF and cohesin cooperatively form compact chromatin loops, leading to the colocalization of gene promoters and their common enhancer in the human *apolipoprotein* gene locus (40). CTCF has been reported to interact with nuclear substructures (71, 72), chromatin remodeling factors (26, 33), RNA polymerase II (10), and CTCF itself (34, 72), as well as undergoing several posttranslational modifications of the protein (12, 29, 37, 70).

Inflammation involves the activation of a highly coordinated gene expression program (43). The tumor necrosis factor (TNF) superfamily members, TNF (initially termed TNF-α), lymphotoxin α (LTα, also termed TNF-β), and lymphotoxin β (LTβ), are major proinflammatory cytokines that mediate inflammatory responses in autocrine/paracrine manners (63). TNF and LTα form homotrimers and act as soluble ligands for the TNF receptor. In contrast, LTβ forms a heterotrimer with LTα and functions as a membrane-bound ligand for the LTβ receptor. In addition to their physiological roles, the aberrant or unbalanced expression of these cytokines is linked to pathological conditions, such as tissue damage/remodeling (38), metabolic diseases (14, 20), and cancer development (19, 23). Hepatic TNF expression is closely related to steatohepatitis (64), and LTβ expression is significantly involved in liver regeneration (3) and hepatocellular carcinomas (HCCs) (23, 67). The *TNF/LT* genes are clustered within the major histocompatibility complex (MHC) class III region on human chromosome 6p21.3, which is the most gene-dense region of the human genome (68). Interestingly, it is reported that NF-κB does not directly interact with the proximal human *TNF* promoter (9, 15, 59) and that NF-κB activation induced by TNF treatment in-

Received 25 October 2011 Returned for modification 1 December 2011
Accepted 7 February 2012
Published ahead of print 21 February 2012
Address correspondence to Mitsuyoshi Nakao, mnakao@gpo.kumamoto-u.ac.jp.
Supplemental material for this article may be found at http://mcb.asm.org/.

doi:10.1128/MCB.06478-11

fluences expression of the *TNF/LT* genes, resulting in the amplified inflammatory response (25). Several DNase-hypersensitive sites, generally suggestive of the presence of regulatory elements, have been found in the *TNF/LT* locus (5, 50, 56, 58). However, a transcriptional mechanism and higher-order chromatin regulation in the human *TNF/LT* locus are unknown.

Investigation of the *TNF/LT* locus identified at least four CTCF/cohesin-enriched insulators and a TNF-responsive TE2 enhancer in human hepatic cells. These CTCF-bound sequences possessed enhancer-blocking activities, and one of the insulators was located between the early-inducible *LTα/TNF* promoters and the late-inducible *LTβ* promoter. Chromosome conformation capture (3C) analyses determined that after TNF stimulation, these CTCF-bound insulators initially associated with the TE2 enhancer and the *LTα*, *TNF*, and *LTβ* promoters, followed by a persistent interaction with the TC3 insulator, the TE2 enhancer, and the *LTβ* promoter. These late-phase interactions were consistent with the formation of a place in which the late-inducible *LTβ* gene was transcriptionally active. TNF stimulation thus induces dynamic changes in higher-order chromatin organization of the overall locus, together with differential expression of the *TNF/LT* genes. Based on our findings that insulators mediate the spatiotemporal control of enhancer-promoter interactions, we propose a dynamic chromatin conformation model and enhancer-blocking mechanism mediated by insulators in the *TNF/LT* locus.

MATERIALS AND METHODS

Cell culture. Hep3B, HCT116, and HeLa cells were cultured in a 1:1 mixture of Dulbecco's modified Eagle's minimum essential medium and Ham's F-12 nutrient medium (DMEM/F12; Sigma) supplemented with 10% (vol/vol) fetal bovine serum (FBS). NeHepLxHT cells were cultured in DMEM/F12 supplemented with 10% (vol/vol) FBS, 10^{-7} M dexamethasone, 10^{-7} M insulin, and 50 μg/ml G418. For TNF stimulation, Hep3B and NeHepLxHT cells were treated with recombinant human TNF-α (210-TA; R&D Systems) at concentrations of 5 ng/ml and 0.5 ng/ml, respectively. For inhibition of NF-κB signaling, BAY11-7082 (10 μM) was added to the medium for 1 h before treatment of the cells with TNF for 0.5 or 1 h.

ChIP and quantitative PCR (qPCR) analysis. Hep3B and NeHepLxHT cells were cross-linked with 1% formaldehyde at 37°C for 10 min. Crude cell lysates were sonicated to generate DNA fragments of 200 to 500 bp. Chromatin immunoprecipitation (ChIP) was performed with anti-CTCF (07-729; Millipore), anti-RAD21 (ab992; Abcam), anti-acetylated histone H3 (06-599; Millipore), anti-acetylated histone H4 (06-866; Millipore), anti-p65 (sc-372; Santa Cruz), anti-p300 (sc-585; Santa Cruz), or anti-RNA polymerase II (phosphor-S5) antibodies (ab5131; Abcam) or with control rabbit IgG (sc-2027; Santa Cruz) (26). Cells were cross-linked for an additional 10 min when anti-p65 and anti-p300 antibodies were used.

DNA enrichment in ChIP samples was determined using qPCR analysis with an ABI Prism 7300 system (Applied Biosystems) and SYBR green fluorescence. The threshold was set to cross a point where PCR amplification was linear, and the cycle number required to reach the threshold was recorded and analyzed using the Microsoft Excel software program. PCR was performed using precipitated DNA and the input DNA. Primer sequences are listed in Table S1 in the supplemental material. Other antibodies used were anti-lamin A/C (sc-7292; Santa Cruz).

Electrophoretic mobility shift assay (EMSA). The CTCF protein was synthesized using a coupled *in vitro* transcription/translation reaction with the TNT T7 Quick system (Promega), according to the manufacturer's protocol. For supershift assays, the reaction mixture was combined with 1 μl anti-CTCF antibodies (612148; BD Biosciences) (40). The sequences of the probes were as follows: H19 DMR, 5′-TGG CAC GGA ATT GGT TGT AGT TGT GGA ATC GGA AGT GGC CGC GCG GCG GCA GTG CAG GCT CAC ACA TCA CAG CCC GAG CCC GCC CCA ACT-3; TC1, 5′-TCT CCA GCA CTT CTT GCT CAG GCA GTA CCC AAA GGG GCC GCC TGG GAG CAG CAG AGA CCA GGC CCA AAG CTG CGG GCT TAC AAC AGG TTA GCC ATC CCA-3′; TC2, 5′-AGA CCC TGG TGT CCT CTC TGG CCT TAT TTA CTC CTG GTC CTC TGC CAG CCC TGC CAC CAG ATG GCC TTC TAA CTC CTT GGT TGA AAG GCC CAT CTC ATT C-3′; TC3, 5′-CCC GGT ACA GAG AGC TGC GCA GCG TGA CCG AGC GG CCC TGG GGG TCC CCG CCG CCA GGG GGC GCC CGG CCC CGG TAG CCG ACG AGA CAG TAG AGG-3′; TC4, 5′-CTT CAC CCA GGT CTC TCC AGA GAG CCT CAG GCC GCT GCC TTT ACT TAG TTC TGT GTT CAA TGC CAG AAT GCT GCC TCC TAC AGG AAG TCC ACC TGT ATT GCC CAC ACC TCC T-3′; negative control, 5′-TGG CAA AAA GAA AGG ACA GGG CTG CAA GGA GAG TAC AGA CAT GTG CTG GTG AGT GCA CTG TCT GCA TAG TTA CAC CAG AGC ATC TTA TCA ATC AGA AAC TTA TC-3′.

Luciferase reporter assay. The reporter vector pIHLE consisted of the *luciferase* gene driven by the mouse *H19* promoter (−818 to +6 from the transcription start site), simian virus 40 (SV40) enhancer, and a 1.8-kb AatII-HindIII fragment containing the *H19* DMR insulator. The plasmid pIHLIE was constructed by inserting the 1.8-kb *H19* DMR fragment between the *luciferase* gene and the enhancer. pIHLTE plasmids were constructed by inserting fragments of about 200 bp, including TC1, TC2, TC3, and TC4, between the *luciferase* gene and the enhancer (pIHLTE-1F/1R, -2F/2R, -3F/3R, and -4F/4R, respectively). For pIHLET, TC fragments were inserted downstream of the enhancer in pIHLE (pIHLET-1F/1R, -2F/2R, -3F/3R, and -4F/4R). To prepare pIHLTE with mutations (pIHLTE-1 M, -2 M, -3 M, and -4 M), base substitutions were introduced in CTCF consensus sequences at the TC1, TC2, TC3, and TC4 sites using a PCR-based mutagenesis method.

The reporter vector pPL consisted of the *SV40* promoter and the *luciferase* gene and is identical to the pGL3-Promoter vector (Promega). pTPL, pAPL, and pBPL contained the *TNF* promoter (−1044 to +54 from the transcription start site), *LTα* promoter (−924 to +43 from the transcription start site), and *LTβ* promoter (−971 to +12 from the transcription start site), respectively, instead of the *SV40* promoter of pPL. TE1 and TE2 sequences were PCR amplified and inserted upstream of pPL, pTPL, pAPL, and pBPL (pTE1-PL, pTE2-PL, pTE1-TPL, pTE2-TPL, pTE2-APL, and pTE2-BPL). The primer sequences used to prepare the TE1 and the TE2 sequences were as follows: TE1-S, CCT GTG GCT GGA TGA AAT CT; TE1-AS, CCT GGG CAA CAA AGT GAG AC; TE2-S, CCA GGG GAG TTG TGT CTG TAA; TE2-AS, GCA GTT CGG TTC CTT GTT CT.

Reporter vectors (0.05 pmol) were transfected into Hep3B cells (1.0×10^5 cells) in a 12-well plate, using FuGene6 reagent (Roche Applied Science), and analyzed using a luciferase reporter assay system (Promega) after 24 h. For dual luciferase activities (26), values are shown as means and standard deviations of the results from at least three independent experiments.

qRT-PCR. Total RNA was isolated from cultured cells with TRIzol (Invitrogen). The cDNA synthesis used 2 μg of total RNAs that was reverse transcribed using a High Capacity cDNA reverse transcription kit (Applied Biosystems), according to the manufacturer's instructions. Quantitative PCR was performed using an ABI Prism 7300 system (Applied Biosystems) and SYBR green fluorescence. Each experiment was performed at least three times. The relative fold enrichment was quantified by normalization to *β-actin* or *glyceraldehyde-3-phosphate dehydrogenase* (*GAPDH*) gene expression. Primer sequences are listed in Table S1 in the supplemental material.

siRNA-mediated knockdown. Small interfering RNAs (siRNAs) for GL3, CTCF, and Rad21 were used as previously reported (40). RELA silencer select validated siRNA (s11914; Ambion) was used for p65 knockdown. siRNAs were transfected using the Lipofectamine RNAiMAX reagent (Invitrogen) for 48 h.

3C assay. For the chromosome conformation capture (3C) assays (21, 52), formaldehyde-cross-linked chromatin from Hep3B and NeHepLxHT cells was digested with DpnII overnight, followed by ligation with T4 DNA ligase at 16°C for 4 h. To prepare control templates for standard curves, a bacterial artificial chromosome spanning the *TNF/LT* locus RPCI11.C-47E16 was digested with Sau3AI, which is insensitive to Dam methylase, followed by random religation. After reversing the cross-links, genomic DNA was purified by phenol extraction and ethanol precipitation. The ligated products were assessed using qPCR with an ABI Prism 7300 system (Applied Biosystems) and Thunderbird SYBR qPCR Mix (Toyobo). The efficiency of DpnII digestion was evaluated after the entire 3C treatment using qPCR to amplify uncut fragments spanning the DpnII site. More than 80% of the individual restriction sites were digested in these experiments. The 3C-qPCR data were normalized to a loading control, using internal primers located in the *TNF/LT* gene locus. We gained similar results after normalization with internal primers located in *GAPDH* (data not shown). The relative frequencies of interactions between the reference and its physically close site in the control state were finally normalized to 1. Examples of the calculation for relative interacting frequencies are described in Results. Statistical analysis was performed using Student's *t* test for the results of more than three independent experiments. Primer sequences are listed in Table S1 in the supplemental material.

Immunofluorescence analysis. Cultured human cells were fixed with 4% paraformaldehyde in phosphate-buffered saline (PBS) for 10 min at room temperature. Fixed cells were rinsed three times in PBS for 5 min and permeabilized with PBS containing 0.2% Triton X-100 and 0.5% normal goat serum (NGS) for 5 min on ice. Cells were rinsed three times in PBS containing 0.5% NGS for 5 min and then incubated with rabbit anti-p65 (sc-372; Santa Cruz) for 60 min followed by secondary donkey Cy3-conjugated or Alexa Fluor 488-conjugated antibodies for 60 min. Labeled cells were washed three times in PBS for 10 min each. Samples were analyzed using a fluorescence microscope system (Orca-ER1394; Olympus).

Patients and histological assessment. A total of 38 patients (male, 29; female, 9) with HCC, who had undergone tumor resection at the National Cancer Center Hospital, Tokyo, Japan, between May 2003 and December 2005, were enrolled in the present study. The median patient age and follow-up period were 63 years and 1,719 days, respectively. Among the 38 HCC patients, 12 were immunologically positive for hepatitis C virus (HCV) infection, and 16 for persistent hepatitis B virus (HBV) infection (hepatitis B virus surface antigen positive), and 10 were negative for both HCV and HBV infection. Histological examination of noncancerous liver tissue samples revealed findings compatible with chronic hepatitis in 22 and cirrhosis in 9 and no remarkable histological findings in 7. The 38 HCCs were histologically classified into 3 well-differentiated, 27 moderately differentiated, and 8 poorly differentiated tumors. All patients were followed for more than 100 days. Clinical and pathological profiles were obtained from the medical records of the patients. This study was approved by the Ethics Committee of the National Cancer Center, Tokyo, Japan, and written informed consent was obtained from all patients.

IHC. Immunohistochemistry (IHC) for TNF and LTβ was performed using a polymer-based method with the Envision+Dual Link system-horseradish peroxidase [HRP] (DK-2600 Glostrup; Dako). Sources and dilutions of primary antibodies were as follows: anti-TNF-α (ab9579), 1:100, Abcam; anti-LTβ (ab64835), 1:50, Santa Cruz Biotechnology. Formalin-fixed, paraffin-embedded serial tissue sections (4 μm) were placed on silane-coated slides for IHC. Sections cut through the maximum tumor diameter were selected for IHC evaluation. The sections were deparaffinized and rehydrated in xylene and grade-diluted ethanol (50 to 100%) and submerged for 20 min in 0.3% hydrogen peroxide with absolute methanol to block endogenous peroxidase activity. Antigen retrieval for TNF and LTβ was carried out by heating in target retrieval solution (Tris-EDTA buffer, pH 9; Dako Cytomation) at 121°C for 10 min by a pressure cooker. After protein blocking, the sections were incubated with each primary antibody at room temperature for 1 h, followed by incubation with Envision+Dual Link reagent at room temperature for 30 min, and visualized using 3,3-diaminobenzidine tetrahydrochloride as a chromogen. Finally, the sections were counterstained with hematoxylin. Sections were gently rinsed in PBS between incubation steps. The primary antibody was omitted from the reaction sequence as a negative control.

All sections were evaluated by two pathologists, Y. Kanai and H. Ojima, with no knowledge of any clinical or pathological information. Immunoreactivities of TNF and LTβ were defined as follows: negative, no cytoplasmic staining was observed or the intensity of cytoplasmic staining was lower than that for noncancerous hepatocytes within the same section in more than 50% of cancer cells; positive, the intensity of cytoplasmic staining was equivalent to or higher than that of noncancerous hepatocytes in more than 50% of cancer cells.

Statistical analysis. Differences between groups were analyzed using Student's *t* test. A *P* value of <0.05 was considered statistically significant.

RESULTS

Distribution of CTCF-enriched sites in the human *TNF/LT* gene cluster. CTCF-enriched sites in the human *TNF/LT* gene region were investigated by checking several genome-wide CTCF-binding profiles available on websites and in our published data (40, 65). At least four CTCF-enriched sites (TC1, TC2, TC3, and TC4) were identified in this locus and were conserved among the cells tested (Fig. 1A; see also Fig. S1A in the supplemental material). There were no probe sets for the TC2 site in genome tiling arrays because of the presence of frequent repeat sequences (shown by asterisks in Fig. S1A in the supplemental material). Interestingly, TC3 was located between the *TNF* and *LTβ* gene promoters, forming the possible boundary between these adjacent chromosomal subregions.

Based on previous reports (28, 69), each TC site contained a 20-bp consensus CTCF-binding motif (Fig. 1B). To determine if CTCF bound directly to these TC sequences, we performed electrophoretic mobility shift assays (EMSAs) using radiolabeled duplex probes of approximately 100 bp for each TC site and the *in vitro* transcribed/translated CTCF protein. Similar to the DMR insulator of the *H19* gene used as a control (40), the TC probes formed complexes with CTCF and were further supershifted by anti-CTCF antibodies. In contrast, negative-control (NC) probes, which had sequences located downstream of the *NFKBIL1* gene, did not bind to CTCF. In addition, competition assays using mutated TC probes carrying base substitutions within the consensus motif showed that mutated probes did not bind to the CTCF protein (see Fig. S1B and C in the supplemental material), indicating that CTCF specifically bound to the TC sequences.

In order to clarify the localization of CTCF and the cofactor cohesin RAD21 in hepatic cells, we performed chromatin immunoprecipitation (ChIP) analyses using anti-CTCF and anti-RAD21 antibodies, followed by quantitative PCR (qPCR) (Fig. 1C and D). We used standard cell lines: Hep3B, which originates from human HCC, and NeHepLxHT, which is a telomerase-immortalized human neonatal hepatocyte line (51). Both CTCF and RAD21 bound to the TC sites but not to the NC site. RAD21 was relatively enriched with CTCF at TC1 in the *TNF/LT* locus. The CTCF enrichment at the TC sites in Hep3B cells may be remarkable due to the high expression of this gene (see Fig. S1D in the supplemental material) compared with that in NeHepLxHT cells.

Differential regulation of *TNF/LT* genes under TNF stimulation. To examine the transcriptional regulation of the *TNF/LT*

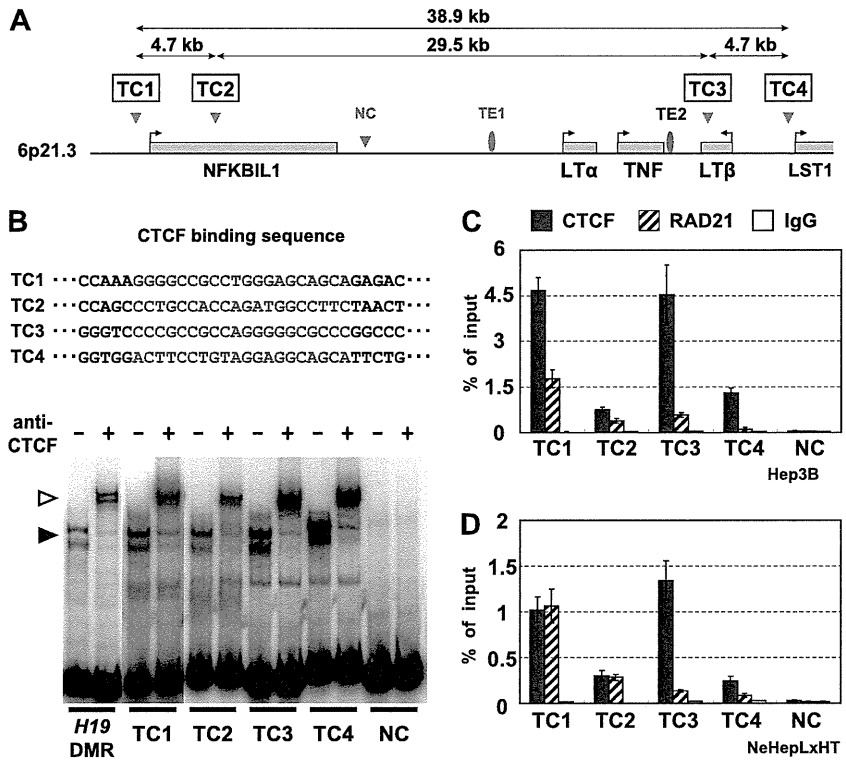

FIG 1 CTCF-enriched sites in the human *TNF/LT* gene cluster locus. (A) CTCF-enriched sites in the *TNF/LT* locus on human chromosome 6p21.3. In addition to the *NFKBIL1*, *LTα*, *TNF*, *LTβ*, and *LST1* genes, a newly identified TE2 enhancer is indicated by a red oval. Based on genome-wide CTCF-binding profiles available from websites and our published data (see Fig. S1A in the supplemental material), four enriched sites were designated TC1, TC2, TC3, and TC4. NC is used as a negative control, and TE1 is a site with no enhancer activity. (B) Direct binding of CTCF to TC sequences. Predicted CTCF-binding sequences within TC1, TC2, TC3, and TC4 sites are indicated, together with the 20-bp consensus motif (red). For EMSAs, radiolabeled duplex probes of approximately 100 bp for each TC site were incubated with anti-CTCF antibodies and synthesized CTCF. Solid and open arrowheads indicate CTCF DNA and the supershifted complexes, respectively. The *H19* DMR insulator and an intergenic unrelated sequence (NC) were used as controls. (C and D) Existence of CTCF and the cofactor cohesin RAD21 at TC sites. Chromatin immunoprecipitation analyses were carried out with anti-CTCF and anti-RAD21 antibodies and control IgG, followed by quantitative PCR with specific primers for each TC site in Hep3B cells (C) or NeHepLxHT cells (D).

genes, we performed quantitative reverse transcription (RT)-PCR (qRT-PCR) analyses with Hep3B and NeHepLxHT cells stimulated by TNF-induced NF-κB activation (Fig. 2A; see also Fig. S2A and B in the supplemental material). Expression of *LTα* and *TNF* mRNAs was markedly increased in Hep3B cells 1 h after stimulation, but *LTβ* mRNA was not simultaneously induced. Moreover, *TNF* expression seemed to be variable after the 1-h peak, while *LTα* and *LTβ* expression did not peak until 24 h after TNF treatment. Early induction of the *LTα* and *TNF* genes also occurred in NeHepLxHT cells, with subsequent expression of the *LTβ* gene. The patterns of *TNF/LT* expression differed between these cell lines, probably due to the constitutively low activation of the NF-κB pathway in Hep3B cells (see Fig. 4A) (11, 55).

Nuclear translocation of NF-κB is critical for its activation (24), and we therefore investigated its subcellular localization under TNF stimulation, using immunofluorescent staining of p65, a subunit of the NF-κB heterodimer (Fig. 2B; see also Fig. S2C in the supplemental material). Cytoplasmic p65 translocated to the nucleus at 30 min after stimulation, and this translocation was inhibited by the addition of BAY11-7082, a specific inhibitor of IκBα phosphorylation (48). The translocated p65 was found to decrease at 1 h after the stimulation (see Fig. S2D in the supplemental material). The expression status of the *TNF/LT* genes was analyzed in parallel using qRT-PCR analyses (Fig. 2C and D). TNF-induced expression of *TNF*, *LTα*, and *LTβ* was attenuated by NF-κB inhibition. Since the use of BAY11-7082 had cytotoxic effects at late time points after TNF stimulation, we carried out siRNA-mediated knockdown of p65 (see Fig. S2G and H in the supplemental material). The induction of the *TNF*, *LTα*, and *LTβ* genes was consistently inhibited by depletion of p65, indicating that the *TNF/LT* genes are regulated by NF-κB in the TNF-treated hepatic cells. Expression of the neighboring *NFKBIL1* gene was unaffected by the stimulation. TNF treatment caused no significant cell damage throughout the study (see Fig. S2E and F in the supplemental material). Thus, the *TNF/LT* genes are differentially induced by TNF-activated NF-κB signaling.

CTCF-dependent enhancer-blocking activity in the *TNF/LT* gene locus. Previous studies demonstrated that the *H19* DMR insulator contains multiple CTCF-binding sites, which are essential for enhancer-blocking activity (6, 22, 26). Luciferase reporter assays were performed with Hep3B cells to test the enhancer-blocking effects of TC1, TC2, TC3, and TC4 (Fig. 3). The presence of TC1, TC2, TC3, and TC4 between the enhancer and promoter reduced the luciferase activities to approximately 60% of those for the control pIHLE vector (pIHLTE-1F, pIHLTE-2F, pIHLTE-3F, and pIHLTE-4F). TC sequences in the opposite direction showed similar results (pIHLTE-1R, pIHLTE-2R, pIHLTE-3R, and pIHLTE-4R), indicating that the TC sites possess enhancer-block-

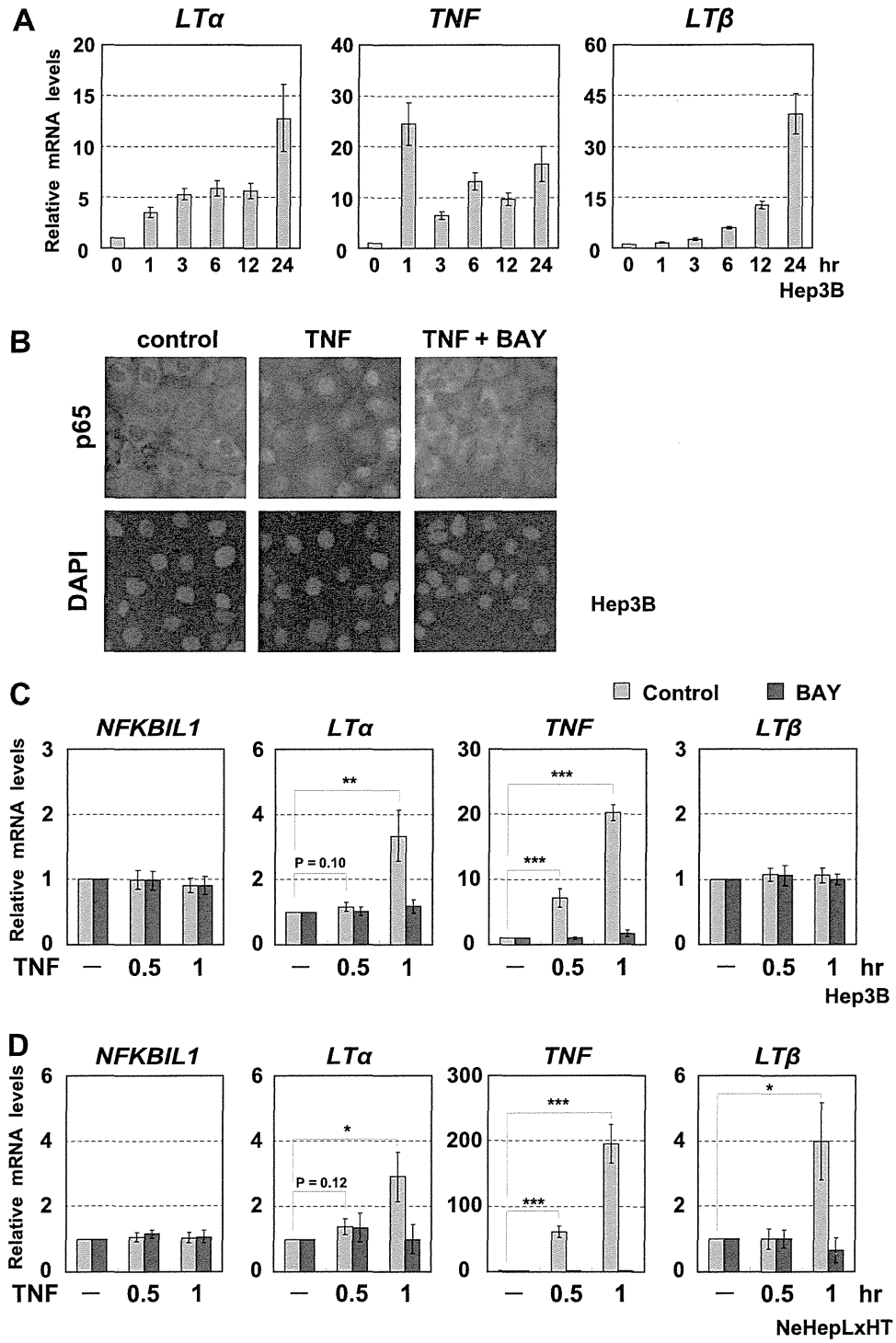

FIG 2 Differential regulation of *TNF/LT* genes under TNF stimulation. (A) Effect of TNF stimulation on *TNF/LT* expression in Hep3B cells. qRT-PCR analyses were performed with Hep3B cells under TNF treatment. (B) Nuclear translocation of NF-κB induced by TNF stimulation. The subcellular localization of the p65 subunit of the NF-κB heterodimer was analyzed by immunofluorescent staining of TNF-stimulated Hep3B cells, together with the use of BAY11-7082, an inhibitor of NF-κB activation. (C and D) NF-κB-dependent expression of the *TNF/LT* genes. TNF-induced expression of the *TNF/LT* genes was examined by qRT-PCR analyses in Hep3B (C) or NeHepLxHT (D) cells in combination with NF-κB inhibition. *, $P < 0.05$; **, $P < 0.01$; ***, $P < 0.005$.

ing activities that are independent of the orientation of the sequences. To exclude the possibility that the TC sites exhibit silencer-like activities, the TC sequences were placed downstream of the enhancer (pIHLET-1F, pIHLET-1R, pIHLET-2F, pIHLET-2R, pIHLET-3F, pIHLET-3R, pIHLET-4F, and pIHLET-4R). Luciferase activity was not reduced by TC sites in this position, suggesting that TC sites do not possess silencer-like functions. The use of mutant TC sites lacking CTCF-binding function, as described

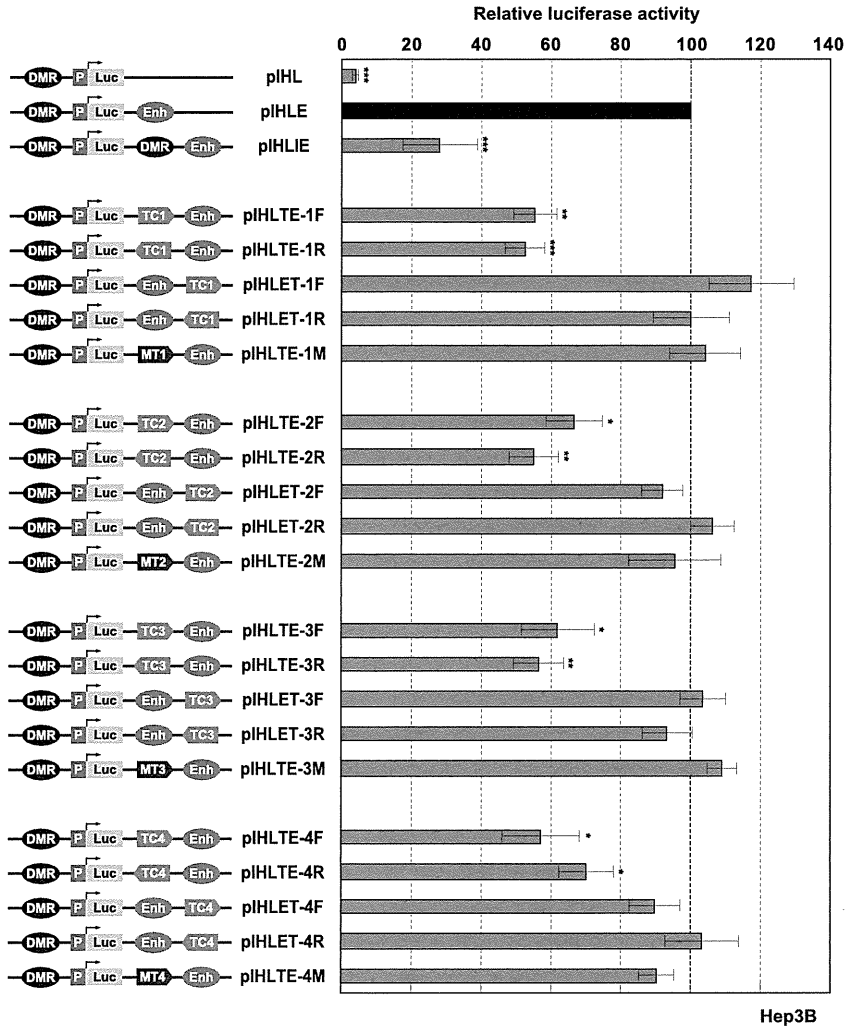

FIG 3 CTCF-dependent enhancer-blocking activity of TC sequences. pIHLTE plasmids were constructed by inserting fragments of approximately 200 bp containing wild-type or mutant-type TC (lacking the CTCF binding function) between the promoter and the enhancer in pIHLE. The *H19* DMR insulator was used as a control. For pIHLET, TC fragments were inserted downstream of the enhancer in pIHLE. The luciferase activities from pIHLE were normalized to 100. The values are given as means and standard deviations of the results from more than three independent experiments. Luc, *luciferase* gene; P, *H19* promoter; Enh, SV40 enhancer; DMR, *H19* DMR insulator; TC1-TC4, CTCF-enriched sites; MT1 to MT4, the mutant TC sequences. *, $P < 0.05$; **, $P < 0.01$; ***, $P < 0.005$.

above (see Fig. S1B and C in the supplemental material), demonstrated no enhancer-blocking effects (pIHLTE-1M, pIHLTE-2M, pIHLTE-3M, and pIHLTE-4M), further suggesting that the insulator activities of the TC sites depend on CTCF. These results suggest that TC1, TC2, TC3, and TC4 are functional insulators.

Characterization of a TNF-responsive hepatic enhancer in the human *TNF/LT* locus. In order to understand the overall regulatory mechanisms in the *TNF/LT* locus, we investigated the role of transcriptional enhancers in hepatic cells. Based on several DNase-hypersensitive sites in the locus (56), modified histones, p300 binding, previously reported enhancers (HSS-9 and HSS+3) in mouse T cells (58), and κB-responsive elements conserved among humans, mice, and rats (30, 31), we chose two candidates, named TE1 and TE2, which were located about 3.5 kb upstream of the *LTα* gene and just downstream of the *TNF* gene, respectively (Fig. 1A; see also Fig. S1A in the supplemental material). Luciferase reporter assays were performed with Hep3B cells to determine if TE1 and TE2 act as enhancers (Fig. 4A). Compared to the control (pPL) and TE1 (pTE1-PL), TE2 significantly increased transcription from the *SV40*, *TNF*, *LTα*, and *LTβ* promoters (pTE2-PL, pTE2-TPL, pTE2-APL, and pTE2-BPL), probably because of the constitutively low activation of NF-κB in Hep3B cells. Under TNF stimulation, these promoter activities were further elevated. These results indicate that TE2 has a TNF-responsive enhancing effect on the *TNF/LT* gene promoters. In addition, the effect of TE2 on the *LTα* promoter seemed to be weaker than that on the *TNF* promoter. The TNF-inducible enhancer activities of TE2 were also detected in other cell lines (see Fig. S3A in the supplemental material).

NF-κB p65 cooperates with histone acetyltransferase p300 (74), which functions as a transcriptional coactivator that accumulates in active enhancer elements (61). To validate the role of TE2 as an active enhancer, we investigated recruitment of p65 and p300 to TE2 by TNF stimulation in Hep3B cells, using ChIP-qPCR assays (Fig. 4B and C). A previously demonstrated enhancer of the *MCP-1* gene (ME) was used as a control (57). Recruitment of p65

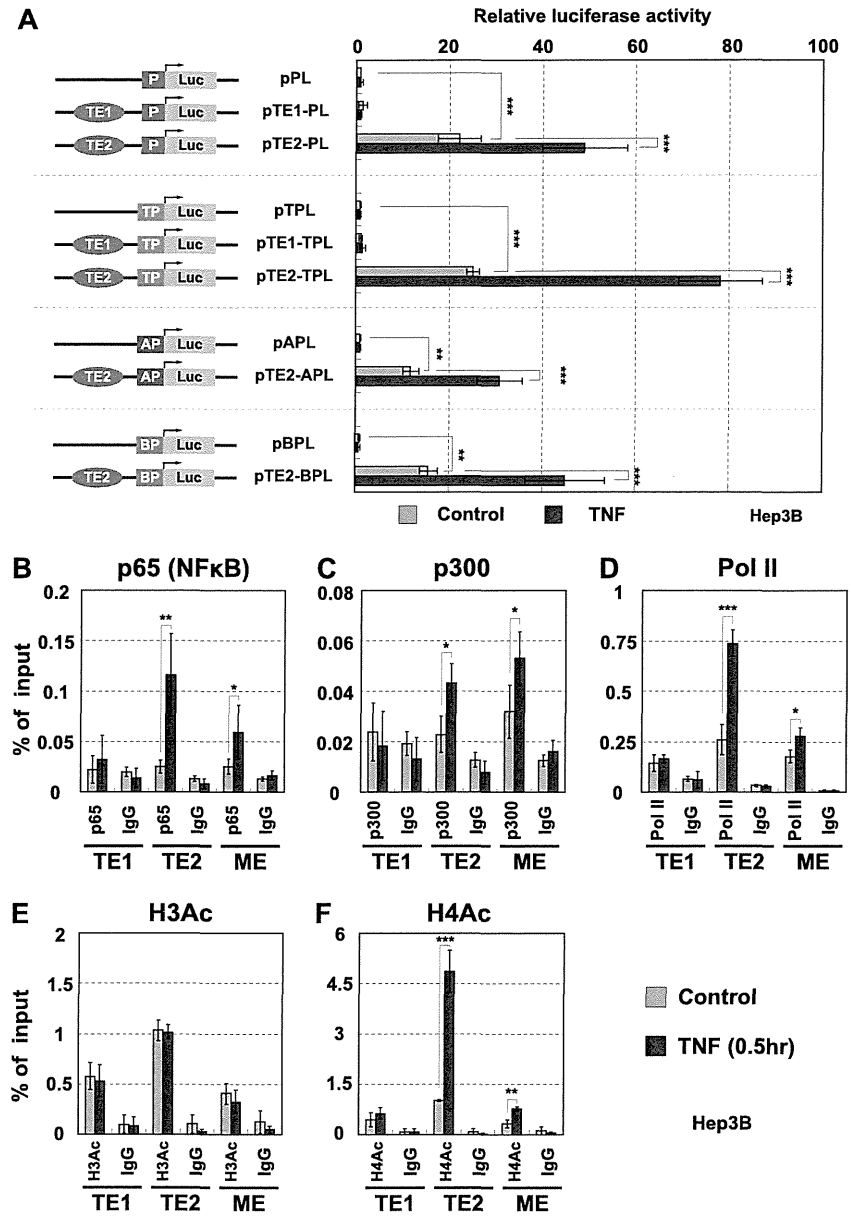

FIG 4 Characterization of TNF-responsive enhancer in the human *TNF/LT* locus. (A) Enhancer activity of TE2. The *luciferase* reporter vectors pPL, pTPL, pAPL, and pBPL contained the *SV40* promoter, *TNF* promoter, *LTα* promoter, and *LTβ* promoter, respectively. The candidate enhancers TE1 and TE2 were inserted in these vectors upstream of the promoter. Hep3B cells were transfected with the reporter vectors and treated with TNF for 3 h (solid bars). Luciferase activities were normalized to basal pPL, pTPL, pAPL, and pBPL. The values are given as means and standard deviations of the results from more than three independent experiments. P, SV40 promoter; TP, *TNF* promoter; AP, *LTα* promoter; BP, *LTβ* promoter. (B to E) The chromatin state of the TE2 enhancer in TNF-stimulated Hep3B cells. ChIP assays were performed with antibodies against p65/NF-κB (B), p300 (C), RNA polymerase II (D), or acetylated histone H3 (E) or H4 (F). The *MCP1* enhancer (ME) was used as a positive control. The values are given as means and standard deviations of the results from more than three independent experiments. *, $P < 0.05$; **, $P < 0.01$; ***, $P < 0.005$.

and p300 to TE2 occurred at 0.5 h after TNF stimulation. Interestingly, RNA polymerase II (Pol II) and acetylated histone H4 were also significantly enriched at TE2 (Fig. 4D to F). In contrast, histone H3 acetylation showed no remarkable changes (Fig. 4E). It was previously reported that various stimuli, such as serum, interleukin 1β (IL-1β), gamma interferon (IFN-γ), and TNF induced the acetylation of histone H4 but not histone H3 (2, 13, 32). Similar data were obtained in NeHepLxHT cells (see Fig. S3B in the supplemental material). These results indicate that TE2 is an active enhancer, which has four putative κB-binding motifs (see Fig. S3C in the supplemental material), under TNF-stimulated conditions in hepatic cells.

CTCF and the cofactor cohesin are involved in transcriptional regulation in the *TNF/LT* gene cluster. RNA interference-mediated knockdown in Hep3B cells was used to determine if CTCF and cohesin, which are enriched at the TC insulators, were involved in transcriptional regulation in the *TNF/LT* locus. Western blot and qRT-PCR analyses showed that CTCF and RAD21

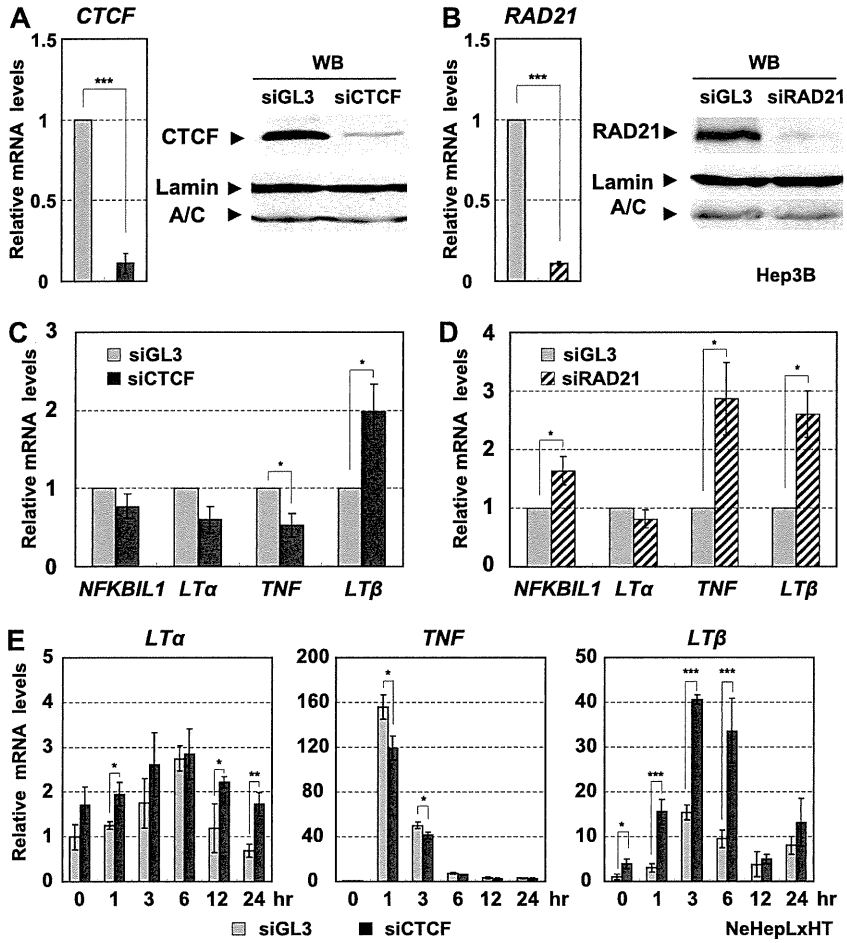

FIG 5 CTCF-mediated insulators are involved in transcriptional regulation in the *TNF/LT* gene cluster. (A and B) RNA interference-mediated knockdown of CTCF (A) and the cofactor cohesin RAD21 (B). Western blot and qRT-PCR analyses were carried out with Hep3B cells. As previously demonstrated (40), more than two distinct siRNAs against CTCF or RAD21 and control siRNAs were used in the experiments. (C and D) Effects of CTCF and RAD21 knockdown on the transcriptional status of the *TNF/LT* genes. Using qRT-PCR analyses, the transcriptional levels of these genes were analyzed relative to that of *β-actin* and were normalized with the control GL3. (E) Effect of CTCF knockdown on *TNF/LT* expression in TNF-stimulated NeHepLxHT cells. CTCF siRNAs were introduced into NeHepLxHT cells for 48 h, followed by TNF treatment for the indicated time period. Values are given as means and standard deviations of the results from more than three independent experiments. *, $P < 0.05$; **, $P < 0.01$; ***, $P < 0.005$.

were depleted at both the protein and RNA levels (Fig. 5A and B). ChIP-qPCR confirmed that the amounts of CTCF and RAD21 were significantly reduced at each TC site in the knockdown cells (see Fig. S4A and B in the supplemental material). The effect of the knockdown on the constitutively low activation of the *TNF/LT* genes in Hep3B cells was tested by qRT-PCR analyses (Fig. 5C and D). The loss of CTCF reduced *TNF* expression and increased *LTβ* expression, while RAD21 depletion increased *NFKBIL1*, *TNF*, and *LTβ* expression, suggesting that CTCF and cohesin have overlapping but certain distinct roles. Indeed, cohesin was reported to be able to behave as a transcriptional regulator, independent of CTCF (46, 54, 65).

We also analyzed the effects of CTCF knockdown on *TNF/LT* genes in TNF-treated NeHepLxHT cells in which the *TNF/LT* genes are normally silenced (Fig. 5E). The loss of CTCF reduced *TNF* expression and accelerated *LTβ* induction in the stimulated cells (Fig. 5E; see also Fig. S4C to 4E in the supplemental material). These results suggest that CTCF/cohesin-mediated insulators are involved in the transcriptional regulation of the *TNF/LT* gene cluster. It is notable, however, that TNF stimulation itself did not affect the degrees of CTCF and RAD21 enrichment at each TC site (see Fig. S4F and G in the supplemental material), suggesting that higher-order chromatin regulation may be involved in the expression of the *TNF/LT* genes upon TNF stimulation. We assessed the knockdown effects with no significant cell damage throughout the study (see Fig. S4H and I in the supplemental material).

Dynamics of higher-order chromatin conformation in the *TNF/LT* locus. 3C assays were performed with Hep3B and NeHepLxHT cells to investigate higher-order chromatin regulation in the *TNF/LT* locus, where TE2 enhancer, gene promoters and TC insulators were identified as functional elements (Fig. 6; see also Fig. S5 in the supplemental material). Use of the 4-bp-recognizing restriction enzyme DpnII allowed us to examine these elements separately. Based on qPCR analyses of the intramolecular ligation products, the relative interacting frequencies of the reference site (yellow bar) with other 7 DpnII fragments containing each element in the *TNF/LT* locus were measured, as further described in Fig. S6 in the supplemental material. TE2 and TC2 were mainly chosen as the reference sites because of their effectiveness in the experiments. The efficiency of DpnII digestion of

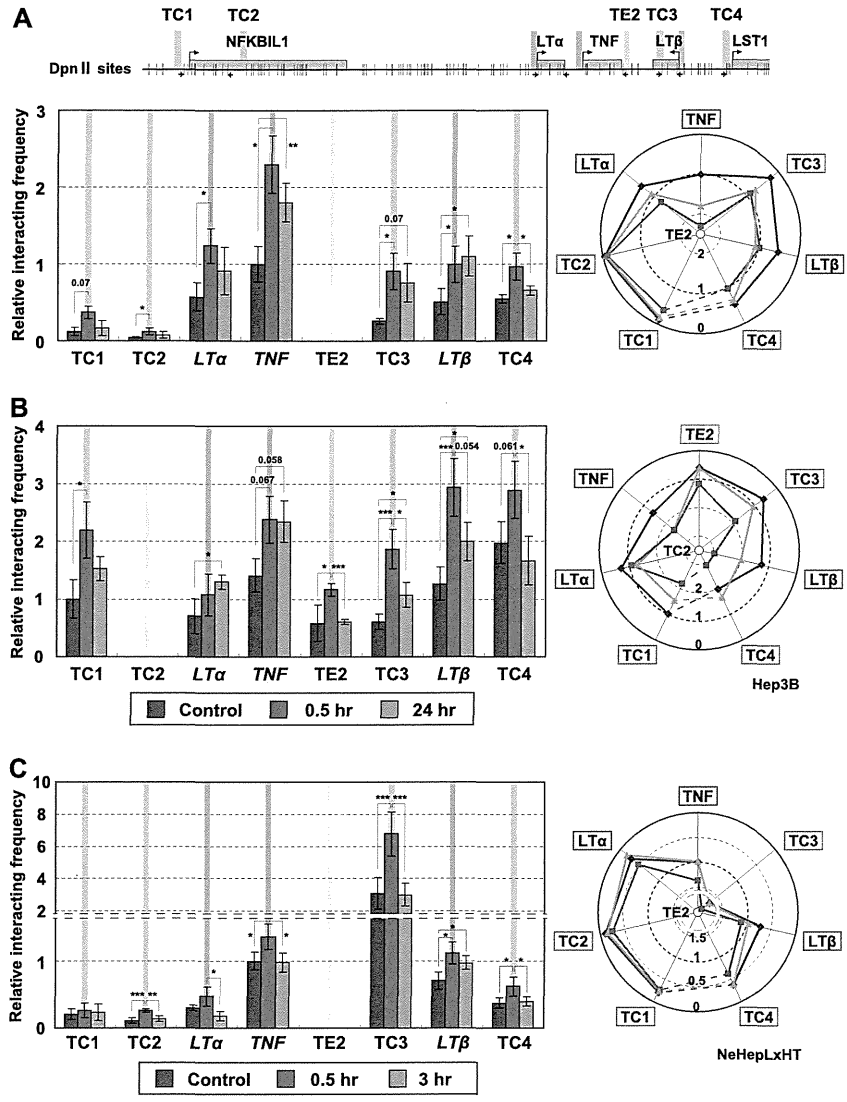

FIG 6 Dynamic changes in higher-order chromatin conformation of the *TNF/LT* locus under TNF stimulation. DpnII digestion was used to design 3C analyses to allow the examination of individual fragments containing each TC site, TNF/LT gene promoter, and TE2 enhancer. (A) The relative interacting frequencies between the reference TE2 fragment (yellow bar) and other DpnII fragments were determined by qPCR analyses of at least three distinct samples from Hep3B cells under TNF treatment. The relative frequencies of interactions between the reference TC2 (yellow bar) and other DpnII fragments in Hep3B cells (B) or between the reference TE2 (yellow bar) and other DpnII fragments in NeHepLxHT cells (C) are shown. In the right panel, the radar chart shows the average relative frequencies of interactions between the reference (central yellow circle) and each functional element. PCR amplification using internal primers located in the *TNF/LT* locus was used for a loading control to normalize the amount of DNA fragments. Efficiencies of DpnII digestion and subsequent ligation were confirmed at each restriction site used. The relative frequencies of interactions between the reference and its physically close site in the control state were normalized to 1 (TE2-*TNF* [A and C] or TC2-TC1 [B]). Control basal state, blue; *TNF*-expressing state, magenta; *TNF/LTβ*-expressing state, green. TC sites, *TNF/LT* gene promoters, and TE2 enhancer are indicated by the same color bars in the locus (upper panel) and the 3C data. The values are given as means and standard deviations of the results from more than three independent experiments. *, $P < 0.05$; **, $P < 0.01$; ***, $P < 0.005$.

individual sites was > 80%, and samples without ligation gave no PCR-amplified products. We determined if CTCF knockdown affected the chromatin conformation of the *TNF/LT* locus in Hep3B cells (see Fig. S5A and B in the supplemental material). Compared with the basal control state, the frequencies of interactions of the referenced TE2 or TC2 with other fragments were mostly reduced to <50% in the CTCF-depleted cells, suggesting that CTCF is involved in the basal conformation of the locus.

To clarify the spatiotemporal chromatin dynamics of the *TNF/LT* locus, we then examined the frequencies of interaction between these regulatory elements under TNF stimulation (Fig. 6). 3C assays were carried out in the cells under the basal control state, *TNF*-expressing state (0.5 h after stimulation), and *TNF/LTβ*-expressing state (24 or 3 h after stimulation). Compared with results for the basal control state, the frequencies of TE2 interaction with other sites tested in the locus were significantly augmented in *TNF*-expressing Hep3B cells (Fig. 6A), suggesting that intrachromosomal interaction occurred in the locus. Interestingly, TE2 maintained an interaction with the *LTβ* promoter and TC3 in the *TNF/LTβ*-expressing state while remaining separate

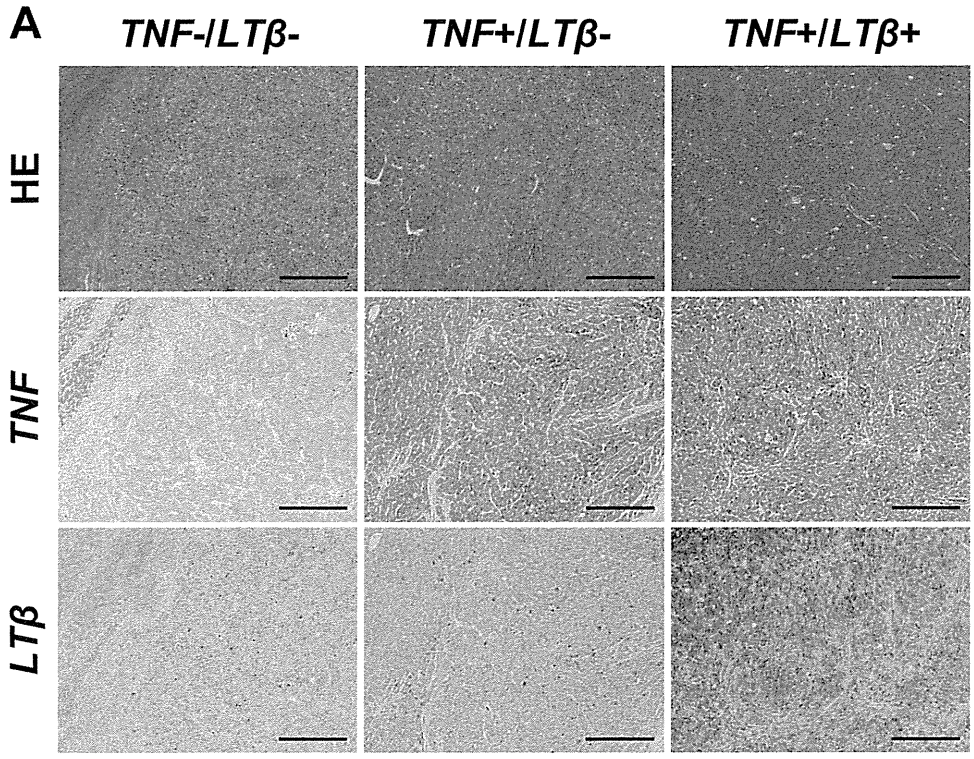

B

TNF \ LTβ	+	-
+	12/38 (31.6 %)	10/38 (26.3 %)
-	0/38 (0 %)	16/38 (42.1 %)

FIG 7 Expression of TNF and LTβ in human hepatocellular carcinoma tissues. (A) Representative immunohistochemical staining of human HCC. When the intensity of cytoplasmic staining was equivalent to or higher than that for noncancerous hepatocytes in >50% of cancer cells, the case was defined as positively stained. Three representative cases of the 38 cancer tissue samples tested are shown. Hematoxylin-and-eosin staining (upper) and immunostaining for TNF (middle) and LTβ (lower) are shown. Scale bar, 500 μm. (B) Percentages of TNF- and LTβ-stained cancer tissues. Cases with neither TNF nor LTβ expression (TNF− LTβ−), expression of both (TNF+ LTβ+), and TNF expression alone (TNF+ LTβ−) were found in 42.1%, 31.6%, and 26.3% of the cancer tissues, respectively. No cases expressed LTβ alone. The data for each tissue are summarized in Table S2 in the supplemental material.

from other elements. We also examined the frequencies of TC2 ligation with other fragments and found that TC2 enhanced the interaction with other fragments in the *TNF*-expressing state (Fig. 6B). However, TC2 maintained its close localization with the *TNF* and *LTα* promoters, but not with other fragments, in the *TNF*/*LTβ*-expressing state. Using the TE2 fragment as a reference, similar data were obtained in TNF-stimulated NeHepLxHT cells (Fig. 6C), except for some interactions of TE2 with the TC3, TC1, and *LTα* promoter. Using the TC2 fragment as a reference, we did not clearly detect the interactions with other fragments in NeHepLxHT cells. Collectively, these data suggest that the enhancer-promoter interactions are selectively controlled by intrachromosomal association and subsequent dissociation of the *TNF*/*LT* locus upon activation of TNF signaling. To further demonstrate interactions between TC insulators in chromatin reorganization, we assessed their relative frequencies of interaction in these cells using TC4 as a reference (see Fig. S5C and D in the supplemental material). These TC sites consistently showed association in the *TNF*-expressing state and subsequent dissociation in the *TNF*/*LTβ*-expressing state (modeled in Fig. S7 in the supplemental material).

Expression of TNF and LTβ in human HCC tissues. To examine whether the expression of TNF and LTβ is differentially regulated *in vivo*, we carried out immunohistochemical (IHC) analyses of HCC tissues (Fig. 7). Immunoreactivities of TNF and LTβ were assessed by comparison with the intensity of cytoplasmic staining of noncancerous hepatocytes within the same section. Representative images are shown in Fig. 7A, and the data for each tissue are summarized in Table S2 in the supplemental material. As summarized in Fig. 7B, neither TNF nor LTβ expression was detected in 16 out of 38 HCCs studied (42.1%), while both were densely stained in 31.6% of the cancer tissues. Interestingly,

TNF alone was highly expressed in 10 of the 38 cancer tissues (26.3%), while LTβ alone was not detected in any cases. There may be at least two transcribed states *in vivo*, a TNF-expressing state and a TNF/LTβ-expressing state. We analyzed the correlation between the IHC data and clinical features and found no significant correlations between TNF and/or LTβ expression status and viral status, histological findings (differentiation grade of cancer, presence of chronic hepatitis or cirrhosis), or overall survival of the patients (data not shown). Although it is currently unknown whether the data for HCC tissues are related to higher-order chromatin states of the *TNF/LT* locus (shown in Fig. 6), these results suggest that differential expression of TNF and LTβ occurs *in vivo*.

DISCUSSION

The present study demonstrates the significance of the spatiotemporal regulation of gene activities and higher-order chromatin dynamics in the human *TNF/LT* locus. We identified four CTCF-dependent insulators (TC1, TC2, TC3, and TC4) and an enhancer (TE2) in hepatic cells. The well-known *H19* DMR insulator contains four CTCF binding sites, while each TC site has single CTCF binding sequence with moderate enhancer blocking activities (Fig. 3). The *LTα/TNF* promoters and TE2 were located between TC2 and TC3, while the *LTβ* promoter was between TC3 and TC4, which may play a role in differential regulation of these three genes. The *LTα/TNF* genes were immediately induced by TNF stimulation in a fashion sensitive to inhibition of NF-κB signaling, while the *LTβ* gene was expressed later, as seen in other cell types (1, 39). Our previous report on the human *apolipoprotein* gene locus suggested that CTCF insulators play an essential role in clustered gene control (40). Furthermore, the current study shows that insulator interactions are likely to mediate intrachromosomal association and subsequent dissociation following TNF signaling. The dynamic enhancer-promoter associations and differential expression in the *TNF/LT* locus may be directed by the NF-κB-related regulatory molecules.

From the viewpoint of enhancer-promoter-insulator associations, we propose a spatiotemporal dynamics model in the human *TNF/LT* locus (see Fig. S7 in the supplemental material). In the basal state, CTCF-bound TC sites, the TE2 enhancer, and the *TNF/LT* promoters are located some distance apart in the chromatin structure. After TNF signaling activation, in the *TNF*-expressing state, the TC insulators, TE2, and *TNF/LT* promoters become colocalized and form a compact chromatin structure, resulting in interactions between TE2 and the *TNF* and *LTα* promoters. Because the *LTβ* gene is not fully induced at this stage, the *LTβ* promoter is likely to be sequestered by forming a possible chromatin loop between TC3 and TC4 (see Fig. S5C and D in the supplemental material). In addition, TC sites may be involved in stabilizing the interaction between TE2 and the *TNF* promoter because of the decrease of *TNF* expression in CTCF-depleted cells (Fig. 5C and E). In the *TNF/LTβ*-expressing state, TE2 significantly maintained its interaction with the *LTβ* promoter despite a reduced association with other elements. Thus, sequential chromatin conformation changes may contribute to switching of the enhancer-promoter interaction. Posttranslational modifications of CTCF and changes in the interacting molecules may be involved in the mechanism of intrachromosomal dynamics in the *TNF/LT* locus (47).

Our study revealed that TNF signaling can induce spatiotemporal remodeling of the clustered gene region and that CTCF insulators are likely to mediate higher-order control of transient enhancer-promoter interactions in the *TNF/LT* locus. Previous studies of the *TNF/LT* locus in hematopoietic cells suggested the presence of certain regulatory elements in intron 3 of the *TNF* gene and in the final exon of the *LTβ* gene (5, 66). The sequences, including the TC3 site, showed silencer activity in human T cells, though our study indicated that TC3 had a CTCF-dependent enhancer-blocking function, suggesting that the regulatory elements may differ among cell types. We showed that CTCF-mediated higher-order chromatin is involved in *TNF/LT* gene regulation. Persistent NF-κB activation in chronic inflammation may result in the chromatin conformation of the *TNF/LT* locus being deregulated and maintained in the *TNF/LTβ*-expressing state as an epigenetic memory. Indeed, constitutive NF-κB activation was recently noted to cause *LTβ* expression in inflamed hepatocytes and HCC cells *in vivo* (35), and *LTβ* was demonstrated to be an inducer of HCC (23). The proposed higher-order chromatin conformation of the *TNF/LT* locus may be involved in these *in vivo* situations.

ACKNOWLEDGMENTS

We thank Hiroyuki Aburatani (The University of Tokyo) for previous collaboration.

This work was supported by grants from the Ministry of Education, Culture, Sports, Science and Technology of Japan, from the Japan Science and Technology Agency (CREST), from the Global Center of Excellence (COE) Cell Fate Regulation Research and Education Unit, Kumamoto University, and from the Naito Foundation (to M.N.).

REFERENCES

1. **Abe K, et al.** 2003. Distinct contributions of TNF and LT cytokines to the development of dendritic cells in vitro and their recruitment in vivo. Blood **101**:1477–1483.
2. **Alberts AS, Geneste O, Treisman R.** 1998. Activation of SRF-regulated chromosomal templates by Rho-family GTPases requires a signal that also induces H4 hyperacetylation. Cell **92**:475–487.
3. **Anders RA, Subudhi SK, Wang J, Pfeffer K, Fu YX.** 2005. Contribution of the lymphotoxin β receptor to liver regeneration. J. Immunol. **175**: 1295–1300.
4. **Barski A, et al.** 2007. High-resolution profiling of histone methylations in the human genome. Cell **129**:823–837.
5. **Barthel R, Goldfeld AE.** 2003. T cell-specific expression of the human TNF-α gene involves a functional and highly conserved chromatin signature in intron 3. J. Immunol. **171**:3612–3619.
6. **Bell AC, Felsenfeld G.** 2000. Methylation of a CTCF-dependent boundary controls imprinted expression of the Igf2 gene. Nature **405**:482–485.
7. **Bell AC, West AG, Felsenfeld G.** 2001. Insulators and boundaries: versatile regulatory elements in the eukaryotic genome. Science **291**:447–450.
8. **Bell O, Tiwari VK, Thomä NH, Schübeler D.** 2011. Determinants and dynamics of genome accessibility. Nat. Rev. Genet. **12**:554–564.
9. **Brinkman BMN, Telliez JB, Schievella AR, Lin LL, Goldfeld AE.** 1999. Engagement of tumor necrosis factor (TNF) receptor 1 leads to ATF-2- and p38 mitogen-activated protein kinase-dependent TNF-α gene expression. J. Biol. Chem. **274**:30882–30886.
10. **Chernukhin I, et al.** 2007. CTCF interacts with and recruits the largest subunit of RNA polymerase II to CTCF target sites genome-wide. Mol. Cell. Biol. **27**:1631–1648.
11. **Chiao PJ, et al.** 2002. Role of Rel/NF-κB transcription factors in apoptosis of human hepatocellular carcinoma cells. Cancer **95**:1696–1705.
12. **Choudhary C, et al.** 2009. Lysine acetylation targets protein complexes and co-regulates major cellular functions. Science **325**:834–840.
13. **Clarke DL, et al.** 2010. TNFα and INFγ synergistically enhance transcriptional activation of CXCL10 in human airway smooth muscle cells via STAT-1, NF-kB and the transcriptional coactivator CREB-binding protein. J. Biol. Chem. **285**:29101–29110.

14. **Cohen JC, Horton JD, Hobbs HH.** 2011. Human fatty liver disease: old questions and new insights. Science **332**:1519–1523.
15. **Falvo JV, Tsytsykova AV, Goldfeld AE.** 2010. Transcriptional control of the TNF gene. Curr. Dir. Autoimmun. **11**:27–60.
16. **Filippova GN, et al.** 1996. An exceptionally conserved transcriptional repressor, CTCF, employs different combinations of zinc fingers to bind diverged promoter sequences of avian and mammalian c-myc oncogenes. Mol. Cell. Biol. **16**:2802–2813.
17. **Gaszner M, Felsenfeld G.** 2006. Insulators: exploiting transcriptional and epigenetic mechanisms. Nat. Rev. Genet. **7**:703–713.
18. **Göndör A, Ohlsson R.** 2009. Chromosome crosstalk in three dimensions. Nature **461**:212–217.
19. **Grivennikov SI, Greten FR, Karin M.** 2010. Immunity, inflammation, and cancer. Cell **140**:883–899.
20. **Gustafson B, Hammarstedt A, Andersson CX, Smith U.** 2007. Inflamed adipose tissue: a culprit underlying the metabolic syndrome and atherosclerosis. Arterioscler. Thromb. Vasc. Biol. **27**:2276–2283.
21. **Hagège H, et al.** 2007. Quantitative analysis of chromosome conformation capture assays (3C-qPCR). Nat. Protoc. **2**:1722–1733.
22. **Hark AT, et al.** 2000. CTCF mediates methylation-sensitive enhancer-blocking activity at the H19/Igf2 locus. Nature **405**:486–489.
23. **Haybaeck J, et al.** 2009. A lymphotoxin-driven pathway to hepatocellular carcinoma. Cancer Cell **16**:295–308.
24. **Hayden MS, Ghosh S.** 2008. Shared principles in NF-kappaB signaling. Cell **132**:344–362.
25. **Hoffmann A, Natoli G, Ghosh G.** 2006. Transcriptional regulation via the NF-κB signaling module. Oncogene **25**:6706–6716.
26. **Ishihara K, Oshimura M, Nakao M.** 2006. CTCF-dependent chromatin insulator is linked to epigenetic remodeling. Mol. Cell **23**:733–742.
27. **Jothi R, Cuddapah S, Barski A, Cui K, Zhao K.** 2008. Genome-wide identification of in vivo protein-DNA binding sites from ChIP-Seq data. Nucleic Acids Res. **36**:5221–5231.
28. **Kim TH, et al.** 2007. Analysis of the vertebrate insulator protein CTCF-binding sites in the human genome. Cell **128**:1231–1245.
29. **Klenova EM, et al.** 2001. Functional phosphorylation sites in the C-terminal region of the multivalent multifunctional transcriptional factor CTCF. Mol. Cell. Biol. **21**:2221–2234.
30. **Kuprash DV, Udalova IA, Turetskaya RL, Rice NR, Nedospasov SA.** 1995. Conserved kappa B element located downstream of the tumor necrosis factor alpha gene: distinct NF-kappa B binding pattern and enhancer activity in LPS activated murine macrophages. Oncogene **11**:97–106.
31. **Kwon J, Lee SJ, Benveniste EN.** 1996. A 3′ cis-acting element is involved in tumor necrosis factor-α gene expression in astrocytes. J. Biol. Chem. **271**:22383–22390.
32. **Lee KY, et al.** 2006. NF-kB and activator protein 1 response elements and the role of histone modifications in IL-1β-induced TGF-β1 gene transcription. J. Immunol. **176**:603–615.
33. **Li T, et al.** 2008. CTCF regulates allelic expression of Igf2 by orchestrating a promoter-polycomb repressive complex 2 intrachromosomal loop. Mol. Cell. Biol. **28**:6473–6482.
34. **Ling JQ.** 2006. CTCF mediates interchromosomal colocalization between Igf2/H19 and Wsb1/Nf1. Science **312**:269–272.
35. **Lowes KN, Croager EJ, Abraham LJ, Olynyk JK, Yeoh GCT.** 2003. Upregulation of lymphotoxin beta expression in liver progenitor (oval) cells in chronic hepatitis C. Gut **52**:1327–1332.
36. **Lutz M, et al.** 2000. Transcriptional repression by the insulator protein CTCF involves histone deacetylases. Nucleic Acids Res. **28**:1707–1713.
37. **MacPherson MJ, Beatty LG, Zhou W, Du M, Sadowski PD.** 2009. The CTCF insulator protein is posttranslationally modified by SUMO. Mol. Cell. Biol. **29**:714–725.
38. **Manzo A, Bombardieri M, Humby F, Pitzalis C.** 2010. Secondary and ectopic lymphoid tissue responses in rheumatoid arthritis: from inflammation to autoimmunity and tissue damage/remodeling. Immunol. Rev. **233**:267–285.
39. **Millet I, Ruddle NH.** 1994. Differential regulation of lymphotoxin (LT), lymphotoxin-beta (LT-beta), and TNF-alpha in murine T cell clones activated through the TCR. J. Immunol. **152**:4336–4346.
40. **Mishiro T, et al.** 2009. Architectural roles of multiple chromatin insulators at the human apolipoprotein gene cluster. EMBO J. **28**:1234–1245.
41. **Mongelard F, Corces VG.** 2001. Two insulators are not better than one. Nat. Struct. Biol. **8**:192–194.
42. **Murrell A, Heeson S, Reik W.** 2004. Interaction between differentially methylated regions partitions the imprinted genes Igf2 and H19 into parent-specific chromatin loops. Nat. Genet. **36**:889–893.
43. **Natoli G, Ghisletti S, Barozzi I.** 2011. The genomic landscapes of inflammation. Genes Dev. **25**:101–106.
44. **Ohlsson R, Renkawitz R, Lobanenkov V.** 2001. CTCF is a uniquely versatile transcription regulator linked to epigenetics and disease. Trends Genet. **17**:520–527.
45. **Ong CT, Corces VG.** 2011. Enhancer function: new insights into the regulation of tissue-specific gene expression. Nat. Rev. Genet. **12**:283–293.
46. **Parelho V, et al.** 2008. Cohesins functionally associate with CTCF on mammalian chromosome arms. Cell **132**:422–433.
47. **Phillips JE, Corces VG.** 2009. CTCF: master weaver of the genome. Cell **137**:1194–1211.
48. **Pierce JW, et al.** 1997. Novel inhibitors of cytokine-induced Ikappa-Balpha phosphorylation and endothelial cell adhesion molecule expression show anti-inflammatory effects *in vivo*. J. Biol. Chem. **272**:21096–21103.
49. **Raab JR, Kamakaka RT.** 2010. Insulators and promoters: closer than we think. Nat. Rev. Genet. **11**:439–446.
50. **Rando OJ, Chang HY.** 2009. Genome-wide views of chromatin structure. Annu. Rev. Biochem. **78**:245–271.
51. **Reid Y, Gaddipati J, Yadav D, Kantor J.** 2009. Establishment of a human neonatal hepatocyte cell line. In Vitro Cell. Dev. Biol. Anim. **45**:535–542.
52. **Splinter E, Grosveld F, de Laat W.** 2004. 3C technology: analyzing the spatial organization of genomic loci in vivo. Methods Enzymol. **375**:493–507.
53. **Sproul D, Gilbert N, Bickmore WA.** 2005. The role of chromatin structure in regulating the expression of clustered genes. Nat. Rev. Genet. **6**:775–781.
54. **Stedman W, et al.** 2008. Cohesins localize with CTCF at the KSHV latency control region and at cellular c-myc and H19/Igf2 insulators. EMBO J. **27**:654–666.
55. **Tay S, et al.** 2010. Single-cell NF-κB dynamics reveal digital activation and analogue information processing. Nature **466**:267–271.
56. **Taylor JM, Wicks K, Vandiedonck C, Knight JC.** 2008. Chromatin profiling across the human tumour necrosis factor gene locus reveals a complex, cell type-specific landscape with novel regulatory elements. Nucleic Acids Res. **36**:4845–4862.
57. **Teferedegne B, Green MR, Guo Z, Boss JM.** 2006. Mechanism of action of a distal NF-κB-dependent enhancer. Mol. Cell. Biol. **26**:5759–5770.
58. **Tsytsykova AV, et al.** 2007. Activation-dependent intrachromosomal interactions formed by the TNF gene promoter and two distal enhancers. Proc. Natl. Acad. Sci. U. S. A. **104**:16850–16855.
59. **Tsytsykova AV, et al.** 2007. Post-induction, stimulus-specific regulation of tumor necrosis factor mRNA expression. J. Biol. Chem. **282**:11629–11638.
60. **van Steensel B.** 2011. Chromatin: constructing the big picture. EMBO J. **30**:1885–1895.
61. **Visel A, et al.** 2009. ChIP-seq accurately predicts tissue-specific activity of enhancers. Nature **457**:854–858.
62. **Vostrov AA, Quitschke WW.** 1997. The zinc finger protein CTCF binds to the APBbeta domain of the amyloid beta-protein precursor promoter. Evidence for a role in transcriptional activation. J. Biol. Chem. **272**:33353–33359.
63. **Ware CF.** 2005. Network communications: lymphotoxins, LIGHT, and TNF. Annu. Rev. Immunol. **23**:787–819.
64. **Watanabe S, Yaginuma R, Ikejima K, Miyazaki A.** 2008. Liver diseases and metabolic syndrome. J. Gastroenterol. **43**:509–518.
65. **Wendt KS, et al.** 2008. Cohesin mediates transcriptional insulation by CCCTC-binding factor. Nature **451**:796–801.
66. **Wicks K, Knight JC.** 2011. Transcriptional repression and DNA looping associated with a novel regulatory element in the final exon of the lymphotoxin-β gene. Genes Immun. **12**:126–135.
67. **Wolf MJ, Seleznik GM, Zeller N, Heikenwalder M.** 2010. The unexpected role of lymphotoxin β receptor signaling in carcinogenesis: from lymphoid tissue formation to liver and prostate cancer development. Oncogene **29**:5006–5018.
68. **Xie T, et al.** 2003. Analysis of the gene-dense major histocompatibility complex class III region and its comparison to mouse. Genome Res. **13**:2621–2636.
69. **Xie X, et al.** 2007. Systematic discovery of regulatory motifs in conserved regions of the human genome, including thousands of CTCF insulator sites. Proc. Natl. Acad. Sci. U. S. A. **104**:7145–7150.

70. **Yu W, et al.** 2004. Poly(ADP-ribosyl)ation regulates CTCF-dependent chromatin insulation. Nat. Genet. **36**:1105–1110.
71. **Yusufzai TM, Felsenfeld G.** 2004. The 5′-HS4 chicken beta-globin insulator is a CTCF-dependent nuclear matrix-associated element. Proc. Natl. Acad. Sci. U. S. A. **101**:8620–8624.
72. **Yusufzai TM, Tagami H, Nakatani Y, Felsenfeld G.** 2004. CTCF tethers an insulator to subnuclear sites, suggesting shared insulator mechanisms across species. Mol. Cell **13**:291–298.
73. **Zhao H, Dean A.** 2004. An insulator blocks spreading of histone acetylation and interferes with RNA polymerase II transfer between an enhancer and gene. Nucleic Acids Res. **32**:4903–4919.
74. **Zhong H, Voll RE, Ghosh S.** 1998. Phosphorylation of NF-κB p65 by PKA stimulates transcriptional activity by promoting a novel bivalent interaction with the coactivator CBP/p300. Mol. Cell **1**:661–671.

Clinical Study

Oncology

Oncology 2012;83:192–200
DOI: 10.1159/000341347

Received: March 7, 2012
Accepted after revision: June 12, 2012
Published online: August 11, 2012

Evaluation of the mRECIST and α-Fetoprotein Ratio for Stratification of the Prognosis of Advanced-Hepatocellular-Carcinoma Patients Treated with Sorafenib

Tomokazu Kawaoka Hiroshi Aikata Eisuke Murakami Takashi Nakahara Noriaki Naeshiro Mio Tanaka Yoji Honda Daisuke Miyaki Yuko Nagaoki Shintaro Takaki Akira Hiramatsu Koji Waki Shoichi Takahashi Kazuaki Chayama

Department of Medicine and Molecular Science, Division of Frontier Medical Science, Hiroshima University, Hiroshima, Japan

Key Words

Hepatocellular carcinoma · Sorafenib · mRECIST · α-Fetoprotein · Child-Pugh score

Abstract

Objective: To compare the assessment of response and prognosis of patients to sorafenib treatment by the Response Evaluation Criteria in Solid Tumors (RECIST), modified RECIST (mRECIST), α-fetoprotein (AFP) and des-γ-carboxy prothrombin (DCP). ***Methods:*** Sixty-six patients with advanced hepatocellular carcinoma (HCC) treated with sorafenib were enrolled in this retrospective study. The response to treatment was evaluated by RECIST, mRECIST and changes in AFP and DCP. ***Results:*** The median survival time of all patients was 8.6 months. The median time to radiological progression was 3.3 months. The response rates [complete response (CR) + partial response (PR)] by RECIST and mRECIST were 3.0 and 9.0%, respectively, while the disease control rates [CR + PR + stable disease (SD)] were 50 and 50%, respectively. Assessment by mRECIST of overall survival provided a better stratification of the patients according to the response to treatment ($p = 0.009$) than RECIST ($p = 0.09$). Assessment of overall survival by a change in AFP ratio of ≤1 at 8 weeks was better than that of >1 at 8 weeks ($p = 0.002$). The DCP ratio was not useful for assessment of overall survival. Multivariate analysis identified mRECIST response (CR + PR + SD; $p = 0.001$), AFP ratio at 8 weeks (≤1; $p = 0.046$) and Child-Pugh A before treatment ($p = 0.012$) as significant and independent determinants of survival. The combination of AFP ratio at 8 weeks, assessment by mRECIST and Child-Pugh score before treatment allows stratification of prognosis of patients treated with sorafenib. ***Conclusion:*** The combination of mRECIST and AFP ratio is useful for the assessment of prognosis of patients with advanced HCC treated with sorafenib.

Introduction

Hepatocellular carcinoma (HCC) is one of the most common malignant tumors worldwide [1–3]. Infection with hepatitis B or C virus (HBV or HCV) is a risk factor for hepatocarcinogenesis. Sorafenib is currently the standard drug for the systemic treatment of patients with advanced HCC who are not candidates for curative treatments such as surgical resection or locoregional therapies

KARGER

Fax +41 61 306 12 34
E-Mail karger@karger.ch
www.karger.com

0030–2414/12/0834–0192$38.00/0

Accessible online at:
www.karger.com/ocl

Hiroshi Aikata, MD
Department of Medicine and Molecular Science, Division of Frontier Medical Science
Programs for Biomedical Research, Graduate School of Biomedical Sciences
Hiroshima University, 1-2-3, Kasumi, Minami-ku, Hiroshima 734-8551 (Japan)
Tel. +81 82 257 5192, E-Mail aikata@hiroshima-u.ac.jp

[4]. This multikinase inhibitor, with activities against Raf kinase and vascular endothelial cell growth factor (VEGF) receptor, has been approved for the treatment of unresectable HCC by the regulatory agencies of the European Union, the USA and other countries [5]. This approval was based on the positive results of a placebo-controlled randomized phase III study of patients with advanced HCC [4]. Subsequently, a phase III study conducted in the Asia-Pacific region, where HBV infection is the predominant etiologic factor for chronic liver disease, has also demonstrated the survival benefits of sorafenib [6].

In general, the Response Evaluation Criteria in Solid Tumors (RECIST) is the standard imaging assessment for evaluation of the response to cancer therapy [7]. However, HCC is a hypervascular tumor. Furthermore, the 2005 American Association for the Study of Liver Diseases practice guideline on the management of HCC stated that evaluation of the treatment response should take into account the induction of intratumoral necrotic areas in estimating the decrease in tumor load, rather than just the reduction in overall tumor size [8]. The major difference between the modified RECIST (mRECIST) and RECIST is the definition of the target lesion; this is no longer the whole lesion, but only the contrast-enhanced portion of the hepatic lesion at the arterial phase of dynamic imaging [5, 9–11]. Sorafenib blocks tumor cell proliferation by targeting the Raf/MEK/ERK signaling at the level of Raf kinase, and has antiangiogenic properties which target VEGF receptor-β tyrosine kinases [5]. Therefore, mRECIST can be used for the assessment of response to treatment, particularly in patients treated with antiangiogenic drugs (similar to RECIST) [11]. However, there have not been many assessment reports about the comparison of response and prognosis evaluated by RECIST and mRECIST regarding sorafenib treatment.

On the other hand, diagnosis and response to the treatment of HCC are currently assessed by various imaging modalities [e.g. ultrasonography, magnetic resonance imaging (MRI) and dynamic computed tomography (CT)] and tumor markers [e.g. α-fetoprotein (AFP) and des-γ-carboxy prothrombin (DCP)] [12–16]. In this regard, the response to therapy and the prognosis for patients with HCC are reported to correlate with changes in AFP (before and after treatment) [17–21]. To our knowledge, however, there is little or no information on the correlation between prognosis and changes in tumor markers and the treatment with sorafenib. This study was designed to compare assessment of the response of patients with advanced HCC to sorafenib treatment by RECIST, mRECIST and changes in tumor markers.

Table 1. Baseline characteristics of all 66 patients treated with sorafenib

Age, years*	63 (35-80)
Gender, male/female	58/8
PS (0/1/2/3)	50/10/2/4
Etiology (HBV/HCV/nonHBVnonHCV)	24/31/11
Child-Pugh (A/B)	58/8
T-bilirubin, mg/dl*	0.8 (0.4–2.7)
Albumin, g/dl*	3.8 (2.5–4.7)
Platelet, $\times 10^4/\mu l$*	13.5 (6.3–30.1)
HCC stage (II/III/IVa/IVb)	3/14/10/39
Barcelona Clinic Liver Cancer Staging Classification (0/A/B/C/D)	2/1/14/49/0
Tumor size, mm	50 (8.3–194)
Number of the tumor (1–2/>3)	16/50
Metastasis, absence/present	28/38
Tumor portal vein thrombus presence/absence	24/42
Relative tumor size (<50%/>50%)	44/22
AFP, ng/ml*	457.4 (<5–2,650,000)
DCP, mAU/ml*	3,702 (18–4,376,200)
Previous therapy (TACE/HAIC/ systemic chemotherapy)	21/16/10

* Median.

Patients and Methods

Patients

The subjects of this retrospective, cohort study were all 66 patients with advanced HCC who had been treated with sorafenib at Hiroshima University between June 2009 and June 2011. These subjects were considered unfit for surgery, liver transplantation, repeat locoregional therapy, repeat transcatheter arterial chemoembolization (TACE) or repeat hepatic arterial infusion chemotherapy (HAIC). The inclusion criteria for treatment with sorafenib were: an Eastern Cooperative Oncology Group performance status (ECOG PS) score of 2 or less, Child-Pugh liver function class A or B, adequate hematologic function (platelet count $\geq 5\times10^4/\mu l$, hemoglobin ≥8.5 g/dl), adequate hepatic function (albumin ≥2.8 g/dl, total bilirubin ≤3 mg/dl and alanine aminotransferase and aspartate aminotransferase ≤5 times the upper limit of the normal range) and adequate renal function (serum creatinine ≤1.5 times the upper limit of the normal range) according to the SHARP study [4].

The clinical characteristics of the study group are summarized in table 1. With regard to treatment received before sorafenib, 19 patients had not received any treatment for HCC, 21 were nonresponders to TACE, 16 were nonresponders to HAIC and 10 were nonresponders to systemic chemotherapy. Tumor staging was based on the Tumor-Node-Metastasis staging system of the Liver Cancer Study Group of Japan [22]: the tumor in patients with stage I had three features; a solitary tumor measuring <2 cm in diameter with no vessel invasion [n = 0], those with stage II fulfilled two of the above three features (n = 3, 5%), while those with

stage III fulfilled one of the above three conditions (n = 14, 21%), stage IVa fulfilled none of the above three, with no distant metastases or intrahepatic condition with lymph node metastases (n = 10, 15%) and those with stage IVb fulfilled none of the above features with distant metastases (n = 39, 59%).

The study was conducted in accordance with the Declaration of Helsinki and the study protocol was approved by the ethics committee of our hospital. Written informed consent was obtained from each participating patient.

Treatment Regimens

All patients commenced treatment with sorafenib between June 2009 and June 2010, at a dose of 400 mg twice daily (standard dose). Treatment interruptions and dose reductions (400 mg once daily) were permitted for adverse drug reactions. Patients continued therapy until death or met one of the following criteria for the cessation of therapy: adverse events that required termination of treatment, deterioration of ECOG PS to 4, worsening liver function or withdrawal of consent. The criteria of liver function for the discontinuation of treatment was when total bilirubin was >3 mg/dl 4 weeks after stopping treatment.

Assessment of Response to Therapy

We defined the minimal treatment duration as 2 months. In patients who continued the treatment for more than 8 weeks, the response to treatment was evaluated by the RECIST and mRECIST at 8 weeks after starting sorafenib therapy. Subsequently, each patient underwent dynamic CT or MRI every 2–3 months. Overall survival was measured from the date of the commencement of sorafenib until the date of death from any cause. The time to radiologic tumor progression was defined as the time from the date of commencement of sorafenib therapy to disease progression, as assessed by RECIST and mRECIST. We defined the minimal time interval for being able to determine stable disease (SD) as 8 weeks.

The concentrations of serum tumor markers AFP and DCP were measured once a month after the start of sorafenib treatment. The AFP ratio was calculated using the following equation: AFP ratio at 8 weeks = AFP value at 8 weeks/AFP value before treatment. The DCP ratio was measured using a similar equation.

Follow-Up Protocol

Safety assessments included the documentation of adverse drug reactions, clinical laboratory tests, physical examination and the measurement of vital signs. Adverse drug reactions were defined according to the Common Terminology Criteria for Adverse Events, version 4.0 (CTCAE v4.0; http://ctep.cancer.gov/protocolDevelopment/electronic_applications/docs/ ctcaev3.pdf).

Statistical Analysis

Continuous variables were represented as mean ± standard deviation, while categorical variables were represented as absolute and relative frequencies. The Mann-Whitney U test was used to compare continuous variables between groups, while categorical variables were compared using the Fisher exact test or its equivalent for more than 2 categories. The time to radiologic tumor progression and the overall survival were calculated by Kaplan-Meier survival curves with log-rank survival comparisons and 95% confidence intervals (95% CI). A Cox proportional hazards model was used to investigate the prognostic factors for overall survival. A p value less than 0.05 denoted the presence of a statistically significant difference. All statistical analyses were carried out with the PASW Statistics 17.0 software (IBM SPSS, Inc., Chicago, Ill., USA).

Results

Sorafenib Treatment

The median duration of treatment was 4.3 (range: 0.1–25.8) months, with a median follow-up period of 6.0 (0.3–25.8) months. Treatment was terminated within 8 weeks in 17 patients (26%) due to progressive disease (PD) in 11 (16%) and adverse effects in 6 (9%). The median overall survival in the 17 patients who stopped the treatment within 8 weeks was 2.1 months, which was significantly shorter than the 10.1 months in the remaining 49 patients who continued the treatment for more than 8 weeks ($p < 0.001$) (fig. 1).

Safety and Tolerability

The drug-related grade 3/4 adverse events encountered in this study were hand-foot skin reactions in 4 (6.0%) patients, diarrhea in 3 (4.5%), general fatigue in 3 (4.5%), deterioration of liver function tests in 3 (4.5%), thrombocytopenia in 2 (3.0%), loss of appetite in 2 (3.0%) and in 1 patient each: hypertension (1.5%), oral ulceration (1.5%), fever (1.5%), perforation of the colon (1.5%) and vomiting (1.5%). As stated above, adverse effects were the reason for the cessation of treatment within 8 weeks in 6 patients. These included worsening of liver function tests in 3 and hand-foot skin reaction in 3 patients.

Efficacy and Response to Treatment

The response to treatment was evaluated by RECIST and mRECIST at 8 weeks from the date of administration of sorafenib. Seventeen patients could not be evaluated because they had died within the 8 weeks or due to worsening of the performance status (PS). Based on RECIST, complete response (CR) and partial response (PR) were each noted in 1 patient and SD was noted in 31. The response rate, defined as the percentage of patients who showed CR or PR, was 3.0%, and the disease control rate was 50%. Based on mRECIST, CR was noted in 2 patients, PR in 4 and SD in 27; the response rate (CR + PR) was 9.0% and the disease control rate was 50% (table 2). One patient evaluated as PR by RECIST was evaluated as CR by mRECIST and 4 patients evaluated as SD by RECIST were evaluated as PR by mRECIST. The median time to radiologic tumor progression was evaluated to be 3.3 months by RECIST and mRECIST (fig. 2a).

Survival

The median survival time of all patients was 8.6 months (fig. 2b). Overall survival according to the response rate evaluated by RECIST and mRECIST are shown in figure 3a, b. One CR patient and one PR patient with RECIST were alive. Two CR patients with mRECIST were alive. The survival rate for PR patients with mRECIST was 76% at 12 months. The prognosis of patients with CR and PR according to RECIST and mRECIST was relatively good. The median survival time of SD patients was 11 months by RECIST and 10 months by mRECIST. The median survival time of PD patients was 5 months by RECIST and mRECIST. Assessment by mRECIST ($p = 0.009$) provided a better stratification of patients according to overall survival, when compared with an assessment by RECIST ($p = 0.09$).

Correlation between Assessment by Tumor Markers and mRECIST

The median AFP ratio at 8 weeks was 1.0. AFP ratio of ≤1 at 4 weeks was noted in 36 of the 66 (54%) patients, while AFP ratio of ≤1 at 8 weeks was noted in 26 of the 66 (39%) patients. The percentages of patients with an AFP ratio of ≤1 at 4 and 8 weeks correlated negatively with the response to treatment. Thus, the percentages of patients with CR + PR with an AFP ratio of ≤1 were high at both 4 and 8 weeks, whereas in SD patients, this percentage decreased from 80 to 62%, at the respective time intervals. Similarly, 53% of PD patients had an AFP ratio of ≤1 at 4 weeks, but the percentage had decreased to only 29% at 8 weeks.

The median of DCP ratio at 8 weeks was 3.0. For the entire group, DCP ratio ≤3 at 4 weeks was noted in 29 of the 66 (43%), but in only 25/66 (37%) at 8 weeks. The DCP ratio at 4 or 8 weeks did not correlate with the mRECIST response at 8 weeks (table 3).

Correlation between Tumor Markers and Survival

There was no significant difference in overall survival between patients with AFP ratio ≤1 and those with >1 at 4 weeks (fig. 4a). However, the overall survival was better for patients with AFP ratio ≤1 at 8 weeks than those with ratio >1 at 8 weeks ($p = 0.002$, fig. 4b). There was no significant difference in overall survival between patients with DCP ratio ≤3 and those with >3 at 4 weeks, nor at 8 weeks (fig. 4c, d).

Prognostic Factors in Patients Treated with Sorafenib

By means of univariate analysis, we then investigated the relationship between survival after the initiation of sorafenib treatment and various clinicopathological variables. Child-Pugh A ($p = 0.001$), AFP ratio at 8 weeks from start of treatment ($p = 0.002$), PS ($p = 0.008$), the mRECIST-determined response to treatment CR + PR + SD ($p = 0.001$) and the continuation of sorafenib treatment >8 weeks correlated significantly with overall survival. The above parameters were then entered into a multiple Cox proportional-hazard model analysis. This identified assessment of overall survival by continuation of sorafenib treatment >8 weeks ($p < 0.001$), mRECIST (CR + PR + SD; $p = 0.029$), AFP ratio at 8 weeks from the start of treatment (<1; $p = 0.011$) and Child-Pugh A ($p = 0.012$) as significant and independent determinants of survival (table 4).

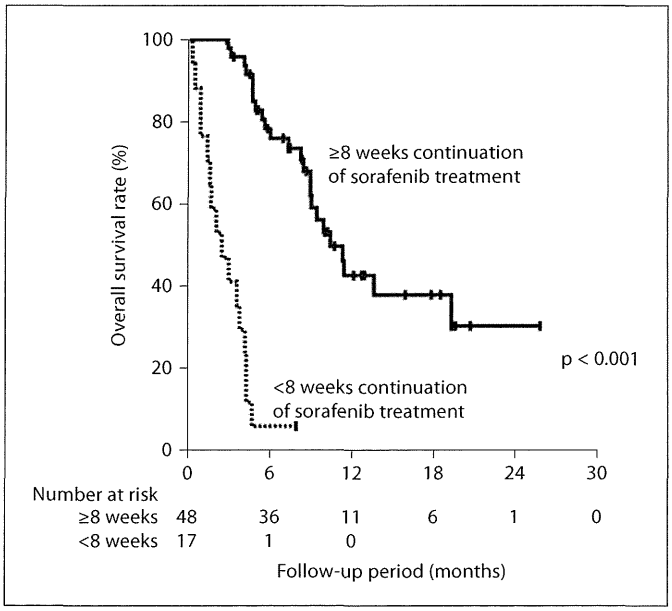

Fig. 1. Overall survival by treatment duration.

Table 2. Response to therapy as assessed by RECIST and mRECIST

	RECIST	mRECIST
CR	1.5 (1)	3 (2)
PR	1.5 (1)	6 (4)
SD	45.4 (30)	39.4 (26)
PD	25.8 (17)	25.8 (17)
Not evaluated	25.8 (17)	25.8 (17)
Response rate: CR + PR	3.0 (2)	9.0 (6)
Disease control rate: CR + PR + SD	50.0 (33)	50.0 (33)

Data are percentage and (number of patients).

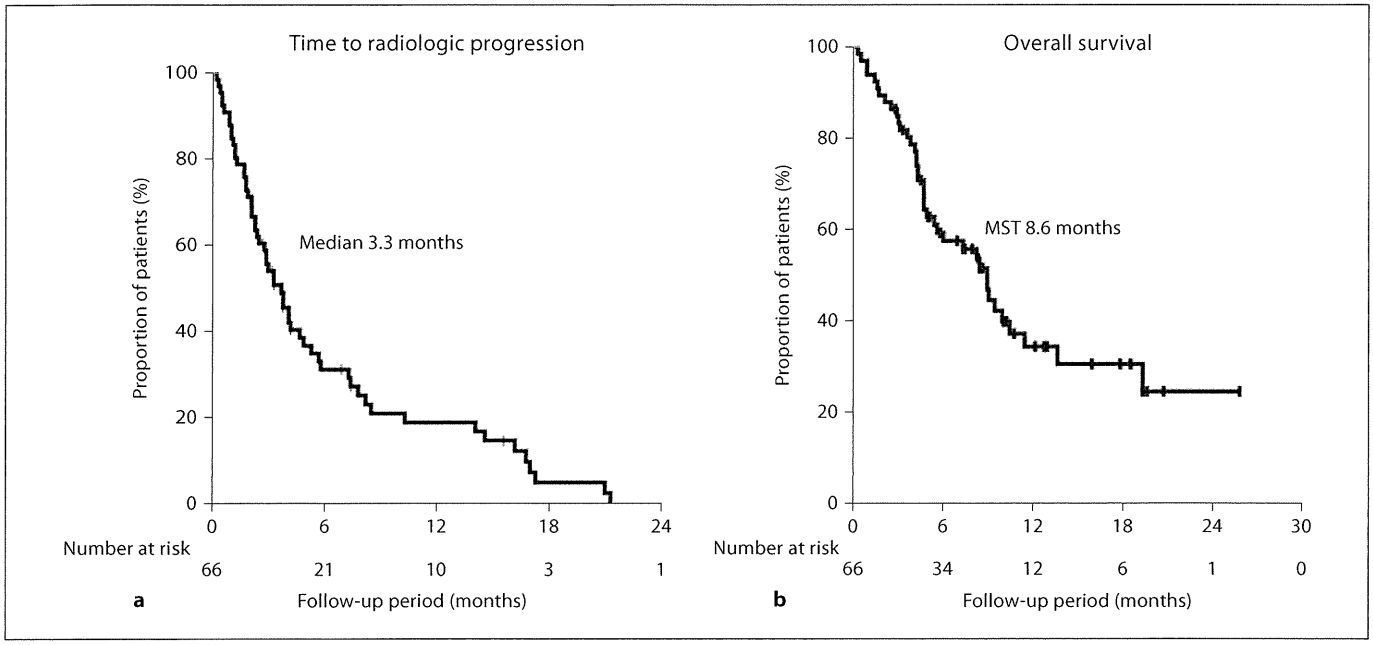

Fig. 2. Time to radiological progression and overall survival rate in sorafenib treatment. **a** The median time to radiological progression was 3.3 months. **b** Median survival time (MST) for all patients was 8.6 months.

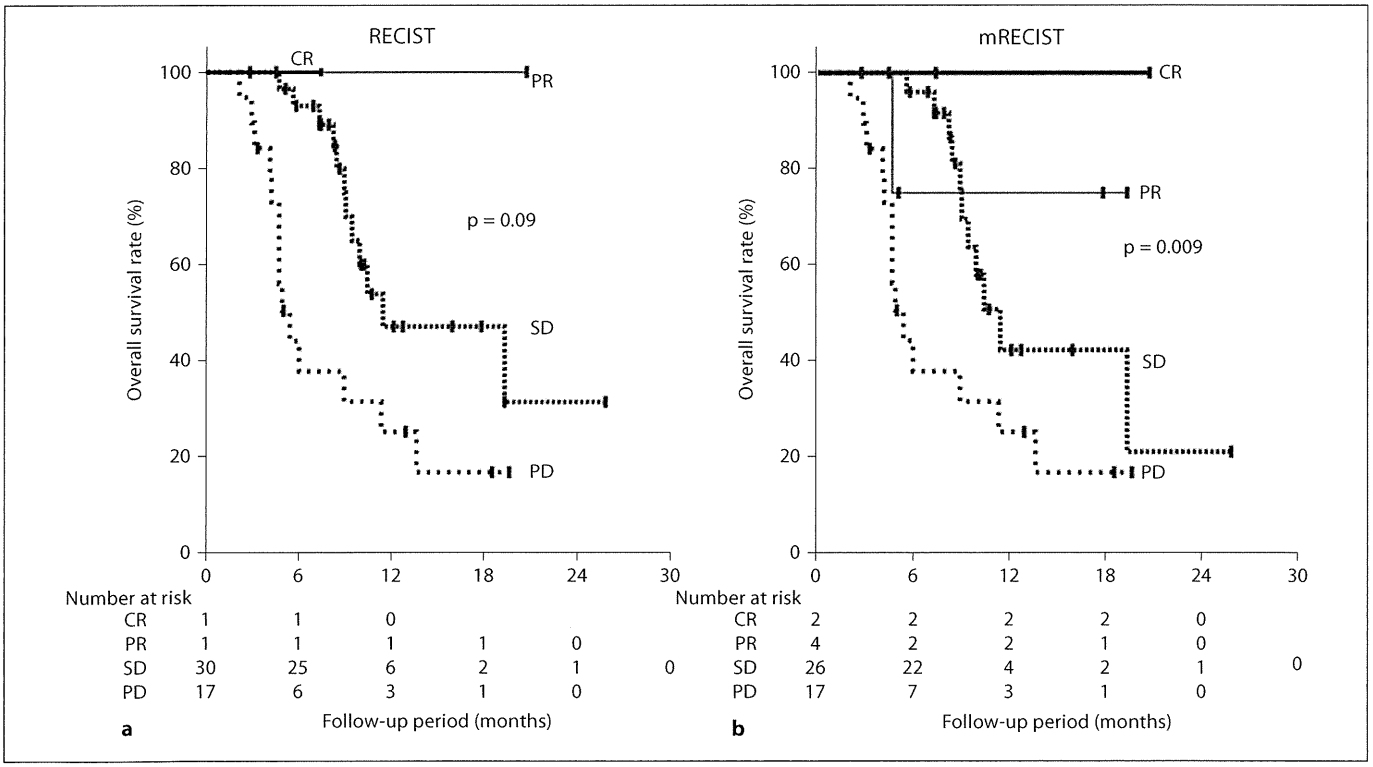

Fig. 3. Overall survival rate by RECIST and mRECIST. **a** Overall survival by RECIST. **b** Overall survival by mRECIST. mRECIST was better than RECIST in the stratification of overall survival according to response to treatment.

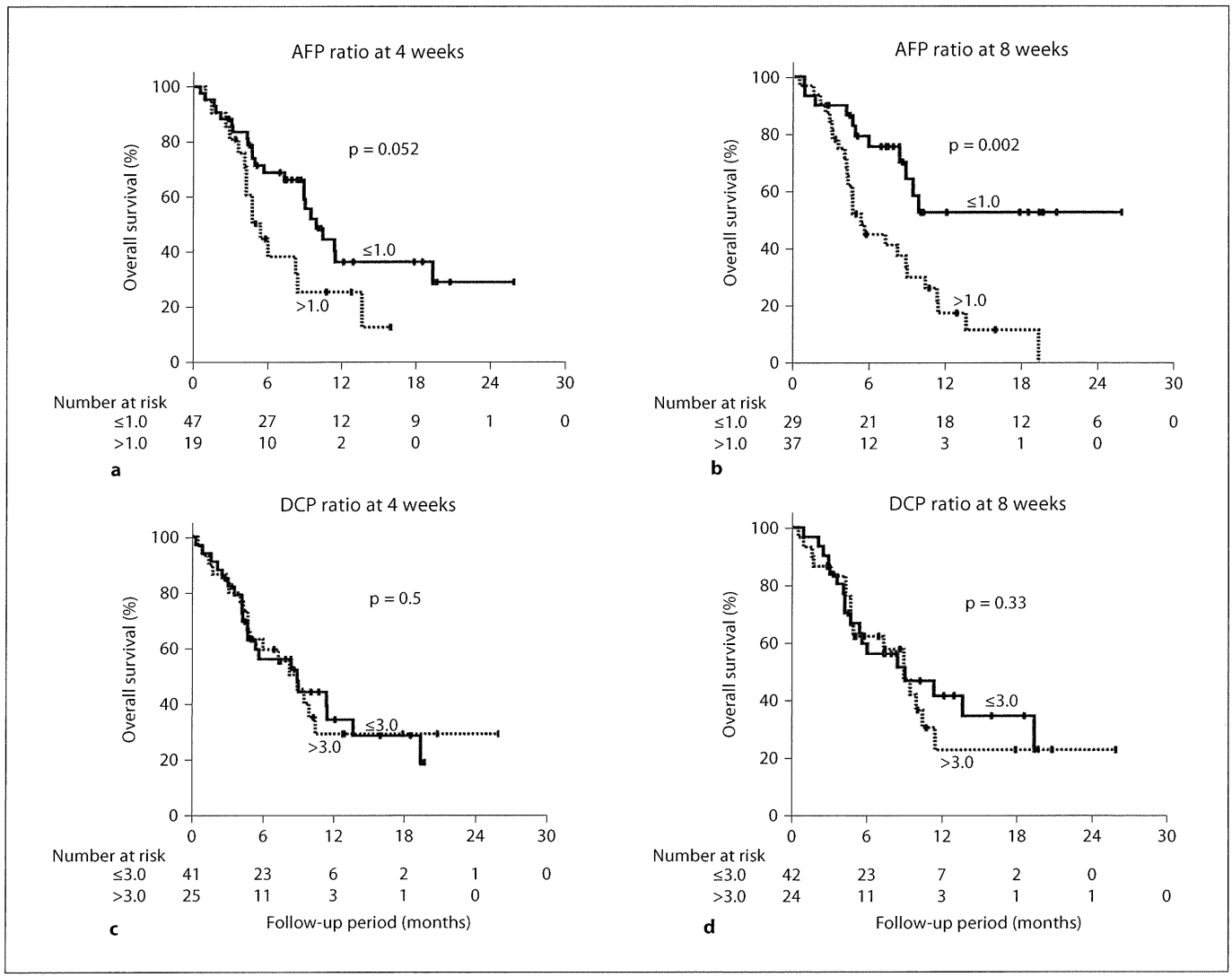

Fig. 4. Correlation between tumor markers and survival rate. **a** Overall survival of patients with AFP ratio ≤1 at 4 weeks and >1 at 4 weeks. **b** Overall survival of patients with AFP ratio ≤1 at 8 weeks and >1 at 8 weeks. **c** Overall survival of patients with DCP ratio ≤3 and >3 at 4 weeks. **d** Overall survival of patients with DCP ratio ≤3 and >3 at 8 weeks.

Table 3. Correlation between tumor marker and mRECIST response

Response by mRECIST at 8 weeks	AFP ratio ≤1 at 4 weeks	AFP ratio ≤1 at 8 weeks	DCP ratio ≤3 at 4 weeks	DCP ratio ≤3 at 8 weeks
CR (n = 2)	100% (n = 2)	100% (n = 2)	50% (n = 1)	50% (n = 1)
PR (n = 4)	100% (n = 4)	75% (n = 3)	50% (n = 2)	50% (n = 2)
SD (n = 26)	80% (n = 21)	62% (n = 16)	65% (n = 17)	54% (n = 14)
PD (n = 17)	53% (n = 9)	29% (n = 5)	53% (n = 9)	47% (n = 8)
Total	54% (36/66)	39% (26/66)	43% (29/66)	37% (25/66)